DEVELOPMENT OF LEAD ALLOYS FOR VALVE-REGULATED LEAD-ACID (VRLA) BATTERIES

A THESIS SUBMITTED TO
THE GRADUATE SCHOOL OF NATURAL AND APPLIED SCIENCES
OF
MIDDLE EAST TECHNICAL UNIVERSITY

BY

ŞAFAK HALICI

IN PARTIAL FULFILLMENT OF THE REQUIREMENTS
FOR
THE DEGREE OF MASTER OF SCIENCE
IN
METALLURGICAL AND MATERIALS ENGINEERING

SEPTEMBER 2010

Approval of the thesis:

DEVELOPMENT OF LEAD ALLOYS FOR VALVE-REGULATED LEAD-ACID (VRLA) BATTERIES

submitted by **ŞAFAK HALICI** in partial fulfillment of the requirements for the degree of **Master of Science in Metallurgical and Materials Engineering, Middle East Technical University** by

Prof. Dr. Canan Özgen
Dean, Graduate School of **Natural and Applied Sciences** _____

Prof. Dr. Tayfur Öztürk
Head of Department, **Metallurgical and Materials Engineering** _____

Prof. Dr. M. Kadri Aydınol
Supervisor, **Metallurgical and Materials Engineering Dept., METU** _____

Examining Committee Members:

Prof. Dr. Tayfur Öztürk
Metallurgical and Materials Engineering Dept., METU _____

Prof. Dr. M. Kadri Aydınol
Metallurgical and Materials Engineering Dept., METU _____

Assoc. Prof. Dr. Zafer Evis
Engineering Sciences Dept., METU _____

Assist. Prof. Dr. H. Emrah Ünalan
Metallurgical and Materials Engineering Dept., METU _____

Dr. Yunus Eren Kalay
Metallurgical and Materials Engineering Dept., METU _____

Date: 13.09.2010

I hereby declare that all information in this document has been obtained and presented in accordance with academic rules and ethical conduct. I also declare that, as required by these rules and conduct, I have fully cited and referenced all material and results that are not original to this work.

Name, Last Name : ŞAFAK, HALICI

Signature :

ABSTRACT

DEVELOPMENT OF LEAD ALLOYS FOR
VALVE-REGULATED LEAD-ACID (VRLA) BATTERIES

Halıcı, Şafak

M.Sc., Department of Metallurgical and Materials Engineering

Supervisor: Prof. Dr. M. Kadri Aydınol

September 2010, 68 pages

In this study, Mg, Sn, Cd, Bi and Sb containing, five binary, three ternary and two quaternary different alloys to be used in a Valve-Regulated Lead-Acid (VRLA) batteries have been studied in terms of their mechanical and electrochemical properties. The investigated properties are hardness, passivity, corrosion rate, hydrogen gassing and the conductivity of the passive film. All electrochemical tests were carried out in 3.75 M H_2SO_4 solution by using open-circuit potential, anodic polarization, polarization resistance measurement and gas collection techniques.

The results showed that while the minimum hardness values were observed in Pb and Pb-Bi alloy, Mg containing alloys have the highest hardness values among all alloys. According to corrosion measurements, lowest $i_{critical}$ value was obtained for Pb, Pb-Bi and Pb-Sn, which reached to passivation region earlier than others. Passive film formation was seen for all specimens. The noble E_{corr} value and minimum corrosion rates belonged to Pb and Pb-Mg. Pb-Bi and Pb-Cd have the highest gas evolution rate. Besides, there were not seen much difference in the gassing behavior of Pb-Sn and Pb-Sb alloys. Mg is found to have a superior

effect on hydrogen gassing. Addition of Sn, as an alloying element, to lead increases the conductivity of the passivation layer. Mg containing alloys did not show good conductivity characteristic. As a result, Mg containing alloy seemed to have an important role because of the desired hardness, corrosion and, gas evolution behavior. However, conductivity of passivation layer of these alloys came up to be low due to the higher tendency of Mg to oxidation. Even so, Mg seems to be a promising alloying element for lead grid alloys in Valve-Regulated Lead-Acid (VRLA) batteries.

Keywords: VRLA batteries, corrosion, hydrogen gassing, PbO conductivity, Pb-Mg alloys.

ÖZ

VALF REGÜLASYONLU KURŞUN-ASİT AKÜLERDEKİ
KURŞUN ALAŞIMLARINI GELİŞTİRİLMESİ

Halıcı, Şafak
Yüksek Lisans, Metalurji ve Malzeme Mühendisliği Bölümü
Tez Yöneticisi: Prof. Dr. M. Kadri Aydınol

Eylül 2010, 68 sayfa

Bu çalışmada, valf-regülasyonlu kurşun asit akülerde kullanılmak üzere Mg, Sn, Cd, Bi and Sb elementlerini içeren, beş tane ikili, üç tane üçlü ve iki tane de dörtlü, farklı alaşım sistemi, mekanik ve elektrokimyasal özelliklerine göre çalışılmıştır. Araştırılan özellikler şunlardır; sertlik, pasiflik, korozyon oranı ve pasif filmin iletkenliğidir. Bütün elektrokimyasal testler 3.75 M H_2SO_4 solüsyonu içerisinde açık devre potansiyel, anodik polarizasyon, polarizasyon direnci yöntemi ve gaz toplama tekniğiyle gerçekleştirilmiştir.

Sonuçlar göstermiştir ki, bütün alaşımlar içerisinde Pb ve Pb-Bi alaşımı minimum sertlik değerine ve Mg içeren alaşımları da en yüksek sertlik değerine sahiptir. Korozyon ölçümlerine göre en düşük $i_{critical}$ değeri diğer alaşımlara nazaran daha erken pasifleşme bölgesine gelen Pb, Pb-Bi ve Pb-Sn alaşımlarında gözükmektedir. Pasif film oluşumu bütün alaşım sistemlerinde tespit edilmiştir. Asal E_{corr} değeri ve minimumu korozyon değeri Pb ve Pb-Mg'ye aittir. Pb-Bi ve Pb-Cd en yüksek gaz salınım değerine sahiptir. Ayrıca, Gaz salınım davranışına göre Pb-Sn ve Pb-Sb arasında çok büyük bir fark yoktur. Mg'nin gaz salınımı üzerine etkisi diğer elementlare kıyasla çok üstündür. Alaşım elementi olarak Sn'ın kurşuna eklenmesi pasif filmin iletkenliğini artırmaktadır. Ancak, Mg içeren alaşımlar iyi bir iletkenlik

karakteristiği göstermemektedir. Sonuç olarak, Mg içeren alaşımlar, elde edilen sertlik, korozyon ve gaz salınım değerlerine göre önemli bir role sahip olduğu gözükmektedir. Fakat Mg'nin oksitlenmeye olan eğilimi yüzünden Mg içeren alaşımların pasif tabakası iletkenliği düşüktür. Buna rağmen, Mg'nin valf-regülasyonlu kurşun asit akülerde gelecek vadeden bir alaşım elementi olduğu görülmektedir.

Anahtar Kelimeler: valf-regülasyonlu kurşun asit akü, korozyon, hidrojen gaz salınımı, PbO iletkenliği, Pb-Mg alaşımları.

.

To My Beloved Rukiye AYAN

and

My Family

ACKNOWLEDGEMENTS

I wish to express my deepest gratitude to my supervisor, Prof. Dr. M. Kadri Aydınol for his guidance, advice, criticism, encouragement and insight throughout the research.

Thanks are to all of my friends at the Department of Metallurgical and Materials Engineering, METU, especially Mine Kalkancı, Atıl Büyükburç, Afshin Izanlou, A. Barış Doğan, Gül İpek Nakaş for their support in the completion of the thesis. Thanks are also to my colleagues in Chamber of Chemical Engineers for their support in the completion of the thesis. I also want to express sincere thanks to Yusuf Yıldırım for his kind interest during Metallography studies.

Besides, thanks to Yiğit Battery Co. for their help about material provision.

Finally, very special thanks to Rukiye Ayan and my parents for their support, encouragement and trust in me throughout my life.

TABLE OF CONTENTS

LIST OF TABLES

TABLES

LIST OF FIGURES

FIGURES

CHAPTER 1

INTRODUCTION

1.1 Battery

Electrical energy has a prominent role in our life; since it can inclusively be applied and easily be converted into light, heat or mechanical energy. A common problem; nonetheless, is that electrical energy can be stored with difficulty. Although capacitors permit its direct storage, their storage densities are not big, compared to require of most applications.

Generally the act of storing electrical energy needs the conversion into other forms of energy [1]. The chemical energy contained in active materials of a battery device is directly converted into electrical energy via reaction of an electrochemical oxidation and reduction (redox). Yet in the matter of a rechargeable system, a reverse process should be followed for the battery to be recharged. The electrons transfer from one material to another by means of an electrical current is involved in this type of reaction [2].

The battery term is often used, whereas the basic electrochemical unit being referred is the cell. A battery composed of one or more of these cells, connected in series or parallel, or both, depending on the desired output voltage and capacity [2].

The three main components included in a cell are:

1. Anode (negative electrode): fuel or reducing electrode that releases electrons to the external circuit and is oxidized throughout the electrochemical reaction.
2. The cathode (positive electrode): the oxidizing electrode that receives electrons from the external circuit and is reduced throughout the electrochemical reaction.
3. The electrolyte: the ionic conductor that supplies the ambient for charge transfer, as ions, inside the cell between the anode and cathode electrode. While the electrolyte is generally

a liquid, such as water or other solvents, with dissolved salts, acids, or alkalis to promote ionic conductivity; solid electrolytes, which are ionic conductors at the operating temperature of the cell are also used in some batteries [2].

In a practical system, the negative electrode is picked out with respect to the following properties in mind; efficiency as a reducing agent, high coulombic output (Ah/g), good conductivity, stability, ease of fabrication, and low cost. The positive electrode must be an efficient oxidizing agent, stable as in contact with the electrolyte, and have a noteful working voltage. Also, electrolyte must have good ionic conductivity but not electronically conductive since this would cause internal short-circuiting [2].

Batteries and electrochemical cells are recognized as primary (nonrechargeable) and secondary (rechargeable), depending on their capability of being electrically charged [2].

Primary batteries are intended to convert their chemical energy into electrical energy only once [1]. They are convenient products having high energy per unit volume (energy density) and good shelf-life (i.e.). They will not significantly discharge when not in use. They are the most widely used batteries, with the main applications in electric torches and electronic equipment. Common examples of this type of battery are zinc-carbon (Leclanché) and alkaline-manganese (zinc-manganese dioxide) cells [3].

Secondary batteries called as reversible energy converters are designed for repeated charge/discharge cycles. They are known as genuine electrochemical storage systems [1]. And they do not need any further cost rather than the initial outlay of the system. The internal combustion engine used as a rechargeable power source for starting, lighting and ignition (SLI) is the most common application. The most well known examples of this type of system are lead-acid and nickel-cadmium batteries [3]. Lithium-ion batteries, composed of lithium containing a lithium metal oxide ($LiMO_2$) as a positive electrode and a lithiated carbon as a negative electrode, are also an important member of secondary batteries. Binder and conductive diluent adhere these materials to a metal foil current collector. Marketing and technology of the lithium-ion battery has rapidly grown in a decade because of its higher specific energy (~ 150 Wh/kg), energy density (~ 400 Wh/L), and rate capability and lower self-discharge (2 % to 8 % per month) than other secondary type of batteries [4, 5].

1.2 History of Lead-Acid Battery

Lead electrodes can be permanently polarized by an external current source. In 1859, a French physician and electrochemist Raymond Gaston Planté found the arrangement that constituted an efficient means of storing energy. In fabrication method of Planté, long rods of lead foil and intermediate layers of coarse cloth or flannel were wound spirally and immersed into a solution of about 10 % sulfuric acid in 1860 for the practical demonstration as it is shown in Figure 1.1 [6].

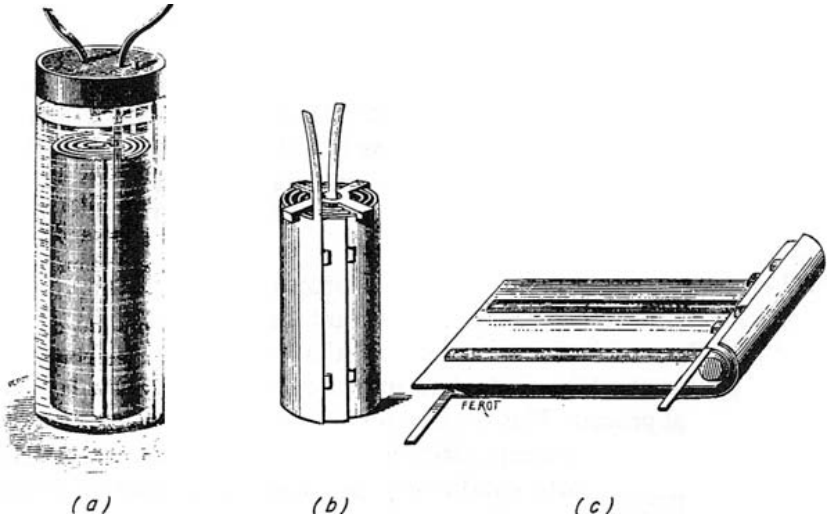

Figure 1.1 Storage battery of Planté with spirally wound electrodes: (a) complete cell, (b) electrode assembly, (c) electrodes with flanel strips during winding [6].

In 1868, the increase in the capacity of this battery could be achieved by longer or repeated charges in a process called forming. Also, Planté recognized that his accumulator could yield appreciably greater currents than the existing primary cells [6].

The next major step in the development of the lead-acid battery was made by Fauré who, in 1881, coated lead foil with lead oxide, but this type of electrode lacked durability. Then, Tudor pasted the oxide on cast ribbed lead plates which were preformed according to the Planté method for better adhesion in 1881 [6].

Moreover, many grid designs were evolved in order to retain active material. At first only perforated or slitted plates were included but later horizontal and vertical or diagonal rods of various cross sections were added. From these earlier designs we have the grid usage. Planté plates are cast from pure lead, while grid plates are cast from alloys that usually contain antimony and often other metallic elements. Antimony apparently was used first by Sellon in 1881. Later in 1955 lead-calcium alloy was introduced by Haring and Thomas. Today the type of grid which is mostly used is cast grids [6].

Lead storage batteries can be classified as conventional type of lead-acid batteries and valve-regulated lead-acid (VRLA) batteries. Conventional lead-acid batteries are “flooded”. That is, the electrolyte is a free liquid to a level above the top of the plates. This type of batteries have the drawback that the cells have to be vented to release the gases which is carrying very fine mist of highly corrosive sulfuric acid and liberated during charging, namely, oxygen at the positive and hydrogen at the negative electrode. The conclusion of this venting is that the batteries should be used only in the upright position; otherwise leakage of sulfuric acid takes place. For many years, scientists have studied to develop sealed batteries which would be safe under all conditions of use and abuse. At first, such attempts revolved around the catalytic recombination of the gases within the battery; yet this approach has not been notably successful. However, invention of VRLA battery brought about the success. In this design, the cell has a starved electrolyte in which the sulfuric acid is immobilized in the separator and the active materials and hence sufficient empty porosity is left for oxygen to diffuse through the separator to the negative plate and recombine back to water. The methods of immobilizing the electrolyte between the plates in VRLA cells are to use gel and absorptive glass micro-fibre (AGM) type electrolytes. The VRLA battery can be set in any orientation, and thus a much greater degree of flexibility is likely to be attained by design engineers.

The development and marketing of VRLA batteries over the last 40 years has rapidly become widespread with so enhanced performance properties which is able to ensure the needs of many new applications thanks to their maintenance-free characteristics, enhanced safety, high-rate capability and high volume efficiency compared with the conventional, flooded-electrolyte batteries [7].

1.3 Physical and Chemical Properties of Lead and Lead Compounds

A lead-acid cell consists of lead dioxide as a positive electrode, sponge lead as a negative electrode and an electrolyte of aqueous sulfuric acid. Lead dioxide is used as the positive active material and metallic lead, in a highly porous surface area structure, as the active material of the negative. Characteristically, both α-PbO_2 (orthorhombic) and β-PbO_2 (tetragonal) are contained in a charged positive electrode. The positive active material is constituted electrochemically from the cured plate. The electrolyte used in the lead acid batteries is a sulfuric acid solution [8].

1.3.1 Lead (Pb)

Pb is naturally occurring element consisting of a mixture of stable isotopes. Its atomic number is 82 and its relative atomic weight is 207.19. The most important ore for the recovery of Pb is galena (PbS). Pb used in the storage battery industry is derived mainly from waste of Pb obtained from reworking the scrap from worn out batteries [6].

Pb is a soft and ductile metal. A freshly prepared surface, for example, obtained by scraping a charged negative plate with a hard object, has a metallic brightness that is to be rapidly lost due to the formation of a grayish oxide layer in air, especially in the presence of water vapor. Finely divided Pb is pyrophoric and can ignite in air at room temperature. The crystal structure of Pb is a face-centered unit cell with its atoms arranged in a cubic close-packed arrangement of spheres and a coordination number of 12 [6].

1.3.2 Lead Oxide (PbO)

Two modifications of PbO are known, the first one is the red tetragonal low-temperature and high-pressure modification (the mineral litharge) and the other is the yellow rhombic high-temperature and low-pressure modification (the mineral massicot) [6].

The storage battery industry uses Pb dust, a powdered PbO manufactured by a thermal process (Barton Oxide); another material produced by an attrition milling process (mill dust) consists mainly of red oxide with a variable content of metallic Pb [6].

1.3.3 Lead Dioxide (PbO_2)

PbO_2 is a nonstoichiometric compound, a powerful oxidizing agent, which is insoluble in H_2SO_4. There are two identified polymorphic crystalline forms of PbO_2: a rhombic form, α-PbO_2 with the columbite-type structure and a tetragonal form, β-PbO_2 with rutile-type structure. α-PbO_2 has more positive equilibrium potential than β-PbO_2 by 0.01 V. Besides, the α form is known to have a larger and more dense crystal morphology which means less electrochemical activity and low capacity per unit weight; yet it is more useful for longer cycle life [2, 6].

1.3.4 Lead Sulphate ($PbSO_4$)

$PbSO_4$ is a nonconductor and has an orthorhombic crystal structure. It is formed on both positive and negative electrodes in the discharge reaction. It may be deposited as very fine grained material or formed in large crystals, known as hard sulphate that resists anodic oxidation to PbO_2 during charge of the plate [6].

1.3.5 Sulfuric Acid (H_2SO_4)

The electrolyte that is used in lead acid batteries is a H_2SO_4 solution, with generally ~ 1,28 specific gravity or 37% acid by weight in a fully charged condition in VRLA batteries. However, specific gravity of electrolyte can be changed in temperature climates between 1.23 and 1.28. Higher concentration electrolytes tend to attack some separators and other components, whereas lower concentrations tend to be insufficiently conductive in a partially charged cell and freeze at low temperatures [8].

The freezing point of aqueous H_2SO_4 solutions varies significantly with concentration. Batteries must therefore be designed in such a way that the electrolyte concentration is above the value at which the electrolyte would freeze when exposed to the anticipated cold. Alternatively, the battery can be insulated or heated so that it remains above the electrolyte freezing temperature [8].

1.4 Chemical Reactions of Lead-Acid Battery

The reaction products at the electrodes on charge and discharge of a lead-acid storage battery are as follows: [8], see Figure 1.2.

Negative electrode:

$$Pb \underset{charge}{\overset{discharge}{\rightleftarrows}} Pb^{2+} + 2e^{-} \tag{1.1}$$

$$Pb^{2+} + SO_4^{2-} \underset{charge}{\overset{discharge}{\rightleftarrows}} PbSO_4 + SO_4^{2-} \tag{1.2}$$

Positive electrode:

$$PbO_2 + 4H^{+} + 2e^{-} \underset{charge}{\overset{discharge}{\rightleftarrows}} Pb^{2+} + 2H_2O \tag{1.3}$$

$$Pb^{2+} + SO_4^{2-} \underset{charge}{\overset{discharge}{\rightleftarrows}} PbSO_4 \tag{1.4}$$

Overall reaction:

$$Pb + PbO_2 + 2H_2SO_4 \underset{charge}{\overset{discharge}{\rightleftarrows}} 2PbSO_4 + 2H_2O \tag{1.5}$$

A dissolution-precipitation mechanism is involved in the basic electrode processes occurring in the positive and negative electrodes, and not a solid-state ion transport or film formation mechanism. The discharge-charge mechanism, known as double-sulfate reaction, is also illustrated in Figure 1.2. When H_2SO_4 in the electrolyte is consumed during discharge, water is produced. The electrolyte is an active material and in definite battery designs can be the capacity-limiting material. As the cell approaches full charge and the majority of the $PbSO_4$ has been converted to Pb or PbO_2, the cell voltage on charge becomes greater than the voltage of gassing (~ 2.39 V per cell) and the overcharge reactions start, resulting in the production of hydrogen and oxygen and the occurrence of water loss [8].

Negative electrode: $$2H^+ + 2e^- \xrightarrow{charge} H_2 \quad (1.6)$$

Positive electrode: $$H_2O + 2e^- \xrightarrow{charge} \frac{1}{2}O_2 + 2H^+ \quad (1.7)$$

Overall reaction: $$H_2O \xrightarrow{charge} H_2 + \frac{1}{2}O_2 \quad (1.8)$$

Any battery, when overcharged, will release hydrogen and oxygen gases in the process of water decomposition. For a battery to be maintenance free, the prevention of gas evolution is compulsory in order to prevent electrolyte exhaustion which would result in devastating failure.

Lead-acid battery designs for many small portable, and some larger fixed applications, have often been referred to as sealed and/or maintenance free. The newer designation for these designs is as a “Valve Regulated Lead-Acid Battery” or VRLA. Containing only a limited amount of electrolyte (“starved” electrolyte) absorbed in a separator or immobilized in a gel is a difference of VRLA from the conventional flooded lead-acid battery designs. VRLA designs have two usual shapes, one with spirally-wound electrodes (jelly-roll construction) in a cylindrical container, and the other with flat plates in a prismatic container. The electrolyte is commonly immobilized by using absorbed electrolyte and gelled electrolyte.

The design and the construction of the VRLA are different from the traditional lead acid battery while the chemistry of both is the same [9]. As the cell is recharged, the primary reaction taking place is as shown in equation (1.9).

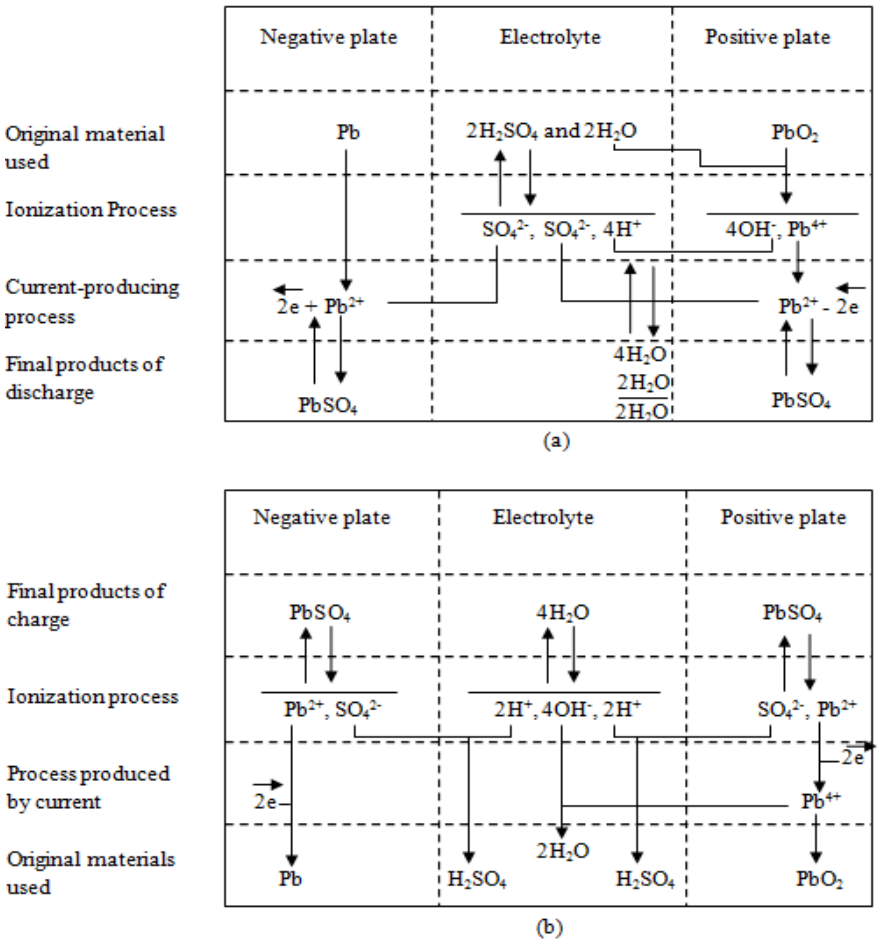

Figure 1.2 Discharge and charge reactions of lead-acid cell: (*a*) Discharge reactions (*b*); Charge reactions [8].

Overall reaction:

$$PbO_2 + Pb + 2H_2SO_4 \underset{\text{charge}}{\overset{\text{discharge}}{\rightleftarrows}} 2PbSO_4 + 2H_2O \qquad E^0 = 2{,}041 \text{ V} \qquad (1.9)$$

The reaction at the positive electrode:

$$PbO_2 + 3H^+ + HSO_4^- + 2e^- \underset{\text{charge}}{\overset{\text{discharge}}{\rightleftarrows}} 2H_2O + PbSO_4 \qquad E^0 = 1{,}685 \text{ V} \qquad (1.10)$$

At the negative electrode:

$$Pb + HSO_4^- \underset{\text{charge}}{\overset{\text{discharge}}{\rightleftarrows}} PbSO_4 + H^+ + 2e^- \qquad E^0 = -0{,}356\ \text{V} \qquad (1.11)$$

The charging source driving current through the battery converts finely divided particles of $PbSO_4$ electrochemically to sponge Pb at the negative electrode and PbO_2 at the positive one. When the cell approaches complete recharge, where the majority of the H_2SO_4 has been converted to Pb and PbO, the overcharge reactions begin. For typical lead-acid cells, the result of these reactions is hydrogen and oxygen gases production and subsequent water loss [10].

A unique aspect of the VRLA design is that the majority of the oxygen generated within the cells at normal overcharge rates is recombined within the cell. Oxygen will react with Pb at the negative plate in the presence of H_2SO_4 as quickly as it can diffuse to the Pb surface, [9]

$$Pb + HSO_4^- + H^+ + \frac{1}{2}O_2 \rightleftarrows PbSO_4 + H_2O \qquad (1.12)$$

This diffusion of gases is a slow process in a flooded type of lead-acid battery, and nearly all the hydrogen and oxygen escape from the cell rather than recombine. On the other hand, in the VRLA battery the closely spaced plates are separated by a glass mat which is composed of fine glass strands in a porous structure [9].

1.5 Failure Modes of Valve Regulated Lead Acid Batteries

In spite of the rapid improvements in performance and design of VRLA batteries, there are still some problems with VRLA battery that are yet to be solved. These failure modes that are probably to affect valve regulated lead acid batteries are given below.

1.5.1 Grid Corrosion

The corrosion of grid materials in VRLA batteries, a serious life-limiting process and also a significant failure mode, leads to various negative effects on different aspects such as functional properties, life and cost of the batteries [11].

In VRLA batteries, it is not possible to submerge the plate poles and other conducting elements in electrolyte and the formation of water diluted wetting layer of acid according to equation (1.13) [12].

$$\frac{1}{2}O_2 + 2H^+ + 2e^- \xrightarrow{charge} H_2O \qquad (1.13)$$

Then the wetting layer potential might be altered to more positive values and the cathodic corrosion protection might be lost. For this reason, drastic corrosion problems have been occurred from time to time at the elements that are conductive in the negative plate [12-13].

Above the positive electrode potential, the rises of the water depletion and the increase in the hydrogen ion concentration take place. Both these events Pb to the increase in the amount of acid around the positive electrode and the corrosion rate [13]. Also, the four-valent ion (Pb^{4+}) is the stable state and constitutes PbO_2. Therefore, grid corrosion in the positive electrode brings about the corrosion of Pb into PbO_2 according to

$$Pb + 2H_2O \xrightarrow{charge} PbO_2 + 4H^+ + 4e^- \qquad (1.14)$$

The produced PbO_2 constitutes a rather compact layer which defends the Pb from further corrosion. The condition at the phase boundary of Pb/PbO_2; nevertheless, is unstable. The corrosion process starts after the breaking of protecting layer. Consequently the corrosion front permeates further step by step into the metal bulk at a quasi-linear rate [12].

1.5.2 Gas Evolution

It is well known that, under normal float conditions, gassing vented from a VRLA battery are mainly oxygen and hydrogen occurring mostly on the surface of the plate material and from the pores walls within the plate material. Hence, it is likely that any surface contamination like impurity elements affects considerably the hydrogen-gassing behaviors of the electrode if the impurities can maintain a lower hydrogen over-potential than Pb [14-15]. Hydrogen and oxygen evolution reactions do harm the valve regulated lead acid battery during charging and discharging processes. Owing to the inefficient recombination reaction, oxygen evolution reaction occurs at 1.23 V, referred to the standard hydrogen electrode (SHE) and so is always exist as a secondary reaction at the positive electrode in the lead acid battery.

Reaction of hydrogen evolution occurs occasionally on the negative electrode in the lead acid battery due to the three reasons, namely: (a) not efficient recombination, (b) positive plate grid corrosion, and (c) oxidation of some organics. Hydrogen oxidation on the negative electrode is generally at a lower rate or in other words less hydrogen is oxidized at the negative electrode, and thus the hydrogen leaves from battery.

The rate at which hydrogen and oxygen venting affects the life of the VRLA battery and also excess gas evolution may lead to the premature loss of battery capacity [12, 14-16].

1.5.3 Grid Growth

The grids are used as a framework and they serve electrical contact to the positive and negative active materials. A stress, caused by this conjoint electrochemical action and concurrent structural role, to the positive plate grids of a lead acid battery is exposed to a corrosion in which Pb is converted into PbO_2 [17]. The corrosion product, PbO_2, requires much higher volume than the Pb. This volume expansion causes mechanical forces in the grid which may become deformed and stretched. This deformation is named as growth.

During the early stages of corrosion, the grid growth was low or unable to be measured but then it gains a steady rate when the corrosion product becomes thicker and the grid member parallely thinner. VRLA batteries can be made to provide some grid growth. However, an

excessive corrosion can result in noticeable grid growth. This causes contact loss between the grid and the active material, and rises to the possibility of short circuits and eventually leading to battery failure [13, 17, 18].

1.5.4 Sulphation of Negative Plate

An important failure mode of VRLA batteries is experienced to be irreversible sulphation of the negative plate, with following loss of capacity. There might be two possible reasons. Firstly, the negative electrode is effectively depolarized by the oxygen recombination reaction so it never attains the low potentials experienced in conventional lead-acid batteries. Secondly, effects of acid stratification can cause irreversible sulphation [13].

1.6 Literature Review

In order to overcome these problems many studies have been conducted. By the help of these studies, some of the problems were solved and some properties of VRLA batteries were improved. Some of the problems of VRLA are corrosion and passivation of the grids. Many studies were done so as to improve corrosion resistance, mechanical properties and evaluate passivation. Some of them are written below;

R. K. Shervedani et al. [19] studied the anodic behavior of Pb-Sn-Ca-Li in 4.5 M H_2SO_4 solution by using many electrochemical methods. Yet; Li was never used as an additive element for the progress of the performance of positive grid materials in lead acid batteries. Therefore, there is no valid information about the effect of Li incorporation in Pb-Sn-Ca alloy. But at the end of their study they reached the conclusion that corrosion resistance of the alloy can be improved by addition of Li. L. Albert and co-workers [20] investigated the effect of addition of Sn (up to the level of 1.2 wt. %) and addition of Ag (up to the level of 0.1 wt. %) to a Pb-0.08 wt. % Ca-0.6 wt. % Sn reference alloy in order to evaluate passivation, corrosion resistance of the grids of lead acid batteries. Next, they used that reference alloy in the processing of fully operative batteries that was tested under cycling conditions. The results are shown below:

- The passivation of Pb-Ca-Sn alloys is lessened by the use of Sn (at a level of 1.2 wt. %) under such conditions that stimulate a deep-discharge, providing the opportunity to increase the conductivity of PbO film formed on the metal surface,

- Using of Ag (at a level of 0.05 wt. %) incread the corrosion resistance of Pb-Ca-Sn alloys under such conditions that stimulate the end-of-charge,

R. Miraglio and co-workers [21] have examined Pb-Ca-Sn alloys so as to determine the role of Sn on the passivation and corrosion phenomenon. They carried out two different experiments; one of which is tested at 1.5 V has showed that the increase of Sn results in greater coarseness in the puzzling structure and the reduction in the grain boundary areas. This induces less weight loss but more deep intergranular corrosion. Only the cast structure is present; that is no discontinuous transformation happens and corrosion occurs mainly at the dendritic boundaries. This leads to an increase in weight loss. On the other hand, PbO is systematically enriched with Sn between the substrate and α-PbO_2. In the second electrochemical test, both the PbO thickness and the doping level of Sn, strongly depend on the Sn content in the alloy. As the Sn content reaches about 1 or 2 wt. % for cast and expanded alloys, respectively, there is a small decrease in the passivation phenomenon. Sn enrichment at the grain boundaries in the cast alloys causes, during the anodization treatment, a local high level of Sn in the lead monoxide. As a conclusion, the amount of Sn that is able to suppress the passivation is slightly decreased. The reduction of Sb content results in deterioration of the mechanical properties and in the cast ability of the alloys but, the addition of small amounts of the other elements such as Se and As can partly compensate this problem. Apart from this, A. Tizpar and Z. Ghasemi [22] investigated the effect of addition of Ag on the corrosion resistance and hydrogen-oxygen evolution of Pb-Sb-As-Se alloys used as positive grids. Their studies have shown that hydrogen evolution rates are inhibited whereas oxygen evolution rates are enhanced by the addition of different concentration of Ag to Pb-Sb-As-Se alloy. W. X. Guo et al. [23] investigated how the addition of various contents of Te (0.01-1.0 wt. %) affects corrosion and oxygen evolution phenomena. At the end of their study they reported that the penetrable corrosion of positive grid alloys might be lessened and also oxygen evolution might be fastened by the use of Te. Another experiment carried out by D. G. Li et al. [26] was about the effects of Ce addition on corrosion behavior of VRLA batteries. According to the experiment results, the corrosion resistance of Pb-Ca-Sn alloy in H_2SO_4 solution can be improved by the addition of Ce. For the improvement of

the corrosion resistance and creeping of strength of maintenance-free electrode, Ag and/or Bi were added to the Pb-Ca-Sn ternary alloy. It's electrochemical and mechanical properties were improved by addition of Ag. However, there is not enough detailed information about micro-structural studies of aged Pb-Ca-Sn-Ag (or Bi) alloys. In the study of I. Mukaitani et al. [27], the precipitation process during aging is observed. The study shows that Bi and Ag addition induce a larger grain size than that in the Pb-Ca-Sn ternary alloys. Grain boundaries are generally prone to corrosion and increasing the grain size is expected to improve corrosion resistance. So, these additives improve the corrosion resistance of Pb-Ca-Sn alloys. Also, retarded discontinuous precipitation, expedited continuous precipitation and hardening are managed by the Ag addition to Pb-Ca-Sn alloys, but it was not the case for Bi. The corrosion of low-Sb Pb-Cd alloys in long–term polarization conditions has been investigated by A. Nuzhny [28]. He studied corrosion resistance of both low-Sb Pb-Cd alloys and Pb-Ca alloy and reported that low-Sb Pb–Cd alloy doped by Ag and Se acquires the remarkable corrosion resistance compared to pure Pb. Furthermore, more compact structure and smaller thickness are seen in films formed at Pb–Sb–Cd–(Se)–(Ag) samples rather than those formed on the other tested alloy samples. E. Jullian et al. [29] investigated the effect of Ba on both negative and positive grids of lead acid batteries. The aim was to get thinner grids at very low cost for negative grids whereas the goal was to produce a more reliable and thinner material for the positive grids. In accordance with these aims, he carried out his studies with increased grid stiffness, stabilized grain structure and also enhanced material reliability provided by using continuous manufacturing processes with addition of Ba. At the end of his study he reached a conclusion that, by adding Ba to Pb-Ca-Sn alloys that can be processed by rolling or continuous casting, both mechanical properties and the corrosion behavior of positive grids can be improved. For negative grids, it was found that improvement in the mechanical properties can lead to thinner grids to a value well below that is possible with a traditional Pb-Ca alloy.

Another main problem of VRLA is gassing evolution; many studies have been done in order to find out how to lessen the volume of gas evolution.

In one of these studies, carried out by L. Guanfa and co-workers [16], the effect of the Ce, a rare earth material, on the behavior of gas evolution of Pb-Ca-Sn alloy is investigated by using cyclic voltammetry, cathodic polarization curves and alternating current (ac) impedance. The finding of this study is that the volume of hydrogen evolution on Pb-Ca-Sn electrode is

more than that on Pb-Ca-Sn-Ce electrode. Furthermore, they claimed that Ce can not only prevent oxygen evolution on Pb-Ca-Sn-Ce electrode surface but, Ce also decrease the water loss observed during charging process and prevent self-discharge occurrence in lead acid battery. So, H. Y. Chen and co-workers [24] studied how the use of Sm as an alloying element influences the electrochemical behavior of pure Pb. Their findings depict that Sm can not only decrease oxygen evolution in VRLA batteries, it can also improve the hardness of the Pb-Ca alloys. Another study in which rare earth element, La, is used is conducted by A. Li et al. [25]. Their aim for this study was to examine the effect of La content on the corrosion and oxygen evolution phenomena. Their findings indicate that the reaction of oxygen evolution is diminished by La existing in the alloys. Moreover, their studies have indicated that corrosion product formed on the Pb-La alloys is not compact and porous that the active materials can easily sit in the voids to efficiently contact the grid surface. Although most of the researchers have focused on the Pb-Bi alloys, the properties of Pb-Bi alloys are not directly related to the properties of Pb-Ca-Sn-Al alloy that was generally used as battery grids. J. Z. Liang et al. [30] investigated the effects of addition of Bi less than 0.05 wt. % on the electrochemical properties such as passivation, corrosion phenomena, oxygen and hydrogen evolution of Pb-Sn-Ca-Al alloys. At the end of their studies, they reported that the Bi addition (0.0108 wt. % - 0.0432 wt. % Bi) enhanced both evolution of hydrogen and oxygen on Pb-Sn-Ca-Al alloys. They also concluded that the conductivity of the Pb-Sn-Ca-Al alloy was improved; the reaction resistance was reduced by the addition of Bi. Lastly, they suggested that the Bi presence may have a positive effect on the constitution of PbO_2. In another study, the effects of Bi on hydrogen evolution reaction on Pb were carried out by Y. M. Wu et al. [31]. The behavior of pure Pb, pure Bi, Pb-Bi alloys and Pb with chemically-deposited Bi was investigated. They reached some results after the investigation of many experiments. They reported that Bi favors hydrogen evolution. Furthermore, Pb with chemically-deposited Bi behaves like Bi in such a way that the Bi that is chemically deposited markedly increases the hydrogen evolution reaction on Pb. In this situation, Bi is harmful to VRLA batteries. On the other hand, Bi in Pb alloys has almost no effect on the evolution of hydrogen reaction that is the alloys act like Pb; consequently Bi is not harmful to VRLA batteries in such a case.

In this study, we aim to get Pb alloys for VRLA batteries which have minimum corrosion and hydrogen gassing evolution rate, also higher hardness behavior and conductive PbO film formed on the grid. Besides, the all properties of alloys of Mg, Bi, Cd and Sn were to

study and investigate. Alloying elements were chosen according to their binary phase diagrams with Pb and their positions in periodic table.

1.7 Phase Diagrams of Binary Alloys

In order to get secondary phase, amount of alloying elements used in this study were determined according to Binary phase diagrams of alloying elements with Pb were given in Figures 1.3 to 1.7.

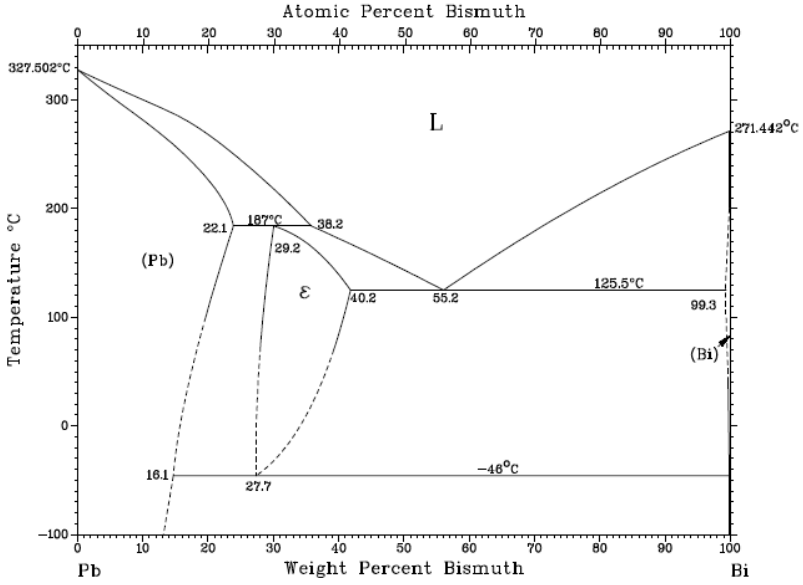

Figure 1.3 Binary Phase Diagram of Pb-Bi [32].

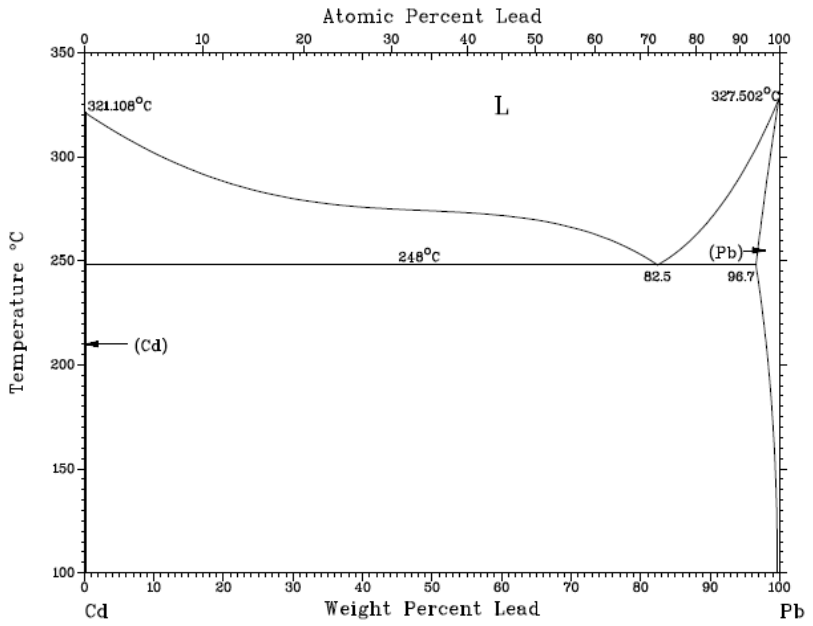

Figure 1.4 Binary Phase Diagram of Pb-Cd [32].

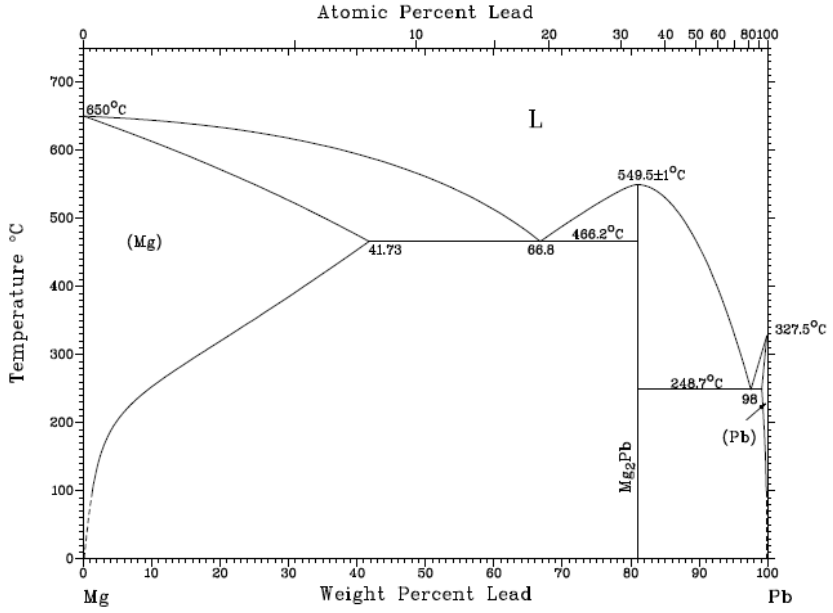

Figure 1.5 Binary Phase Diagram of Pb-Mg [32].

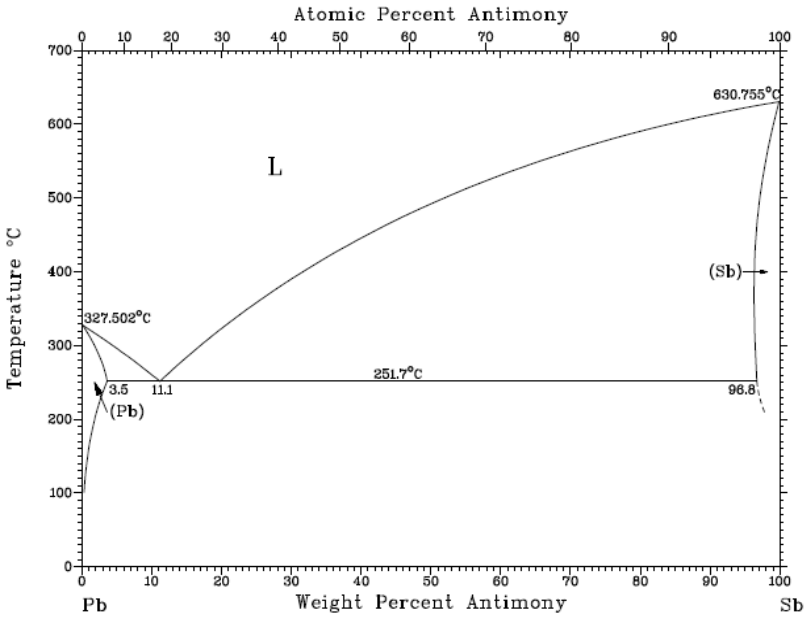

Figure 1.6 Binary Phase Diagram of Pb-Sb [32].

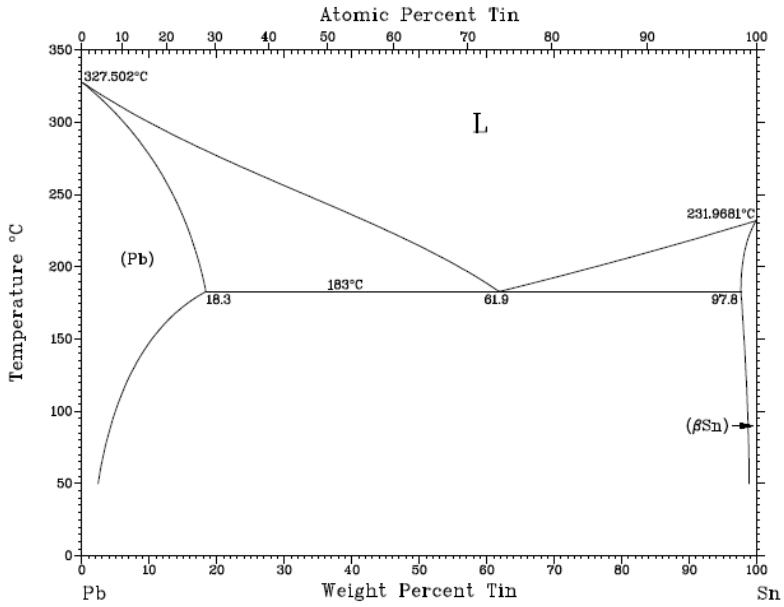

Figure 1.7 Binary Phase Diagram of Pb-Sn [32].

CHAPTER 2

BASICS OF CORROSION

2.1 Introduction to Corrosion

Corrosion is the destructive attack of a metal by chemical or electrochemical reaction with its environment no matter the environment is liquid, gas or hybrid soil-liquid. These environments are named as electrolytes because of their own conductivity for the transfer of an electron. An electrolyte solution might be thought as conductive containing negatively and positively charged ions, namely cations and anions, respectively. Thus, the corrosion process that can be chemical in nature or electrochemical because of a current flow occurs as long as at least two reactions in a particular corrosive environment occur [33, 34]. These reactions are identified as anodic and cathodic reactions and are given below [35]

Anodic process: $M \rightarrow M^{+z} + ze^{-}$ Metal Oxidation (2.1)

Cathodic process: $zH^{+} + ze^{-} \rightarrow H_2$ Hydrogen Evolution (2.2)

$M^{+z} + ze^{-} \rightarrow M$ Metal Reduction (2.3)

For corrosion to take place, the presence of both anodic and cathodic processes is necessary. Corrosion processes are controlled by both thermodynamics and kinetics which are related to the fundamental feasibility of the reaction and the rate, respectively. The thermodynamic possibility of a reaction can be calculated by the free energy change (ΔG) relationship, the electrochemical (or cell) potential of a reaction, E or E_{corr}, at equilibrium is described by the following equation [34, 36].

$$\Delta G = -zFE_{corr} \tag{2.4}$$

where z is the number of electrons present in the reaction, and F is the Faraday's constant. The electrochemical potential of a reaction, E_{corr}, is the algebraic sum of the half-cell reaction potentials of anodic and cathodic reactions, defined as E_a and E_c, respectively. Since E_{corr} is defined to be positive for a spontaneous reaction, equation (2.4) correctly expresses a decrease in Gibbs function, which is the thermodynamic criterion for a spontaneous reaction at constant temperature, T and pressure, P. When determining the spontaneous direction of an electrochemical reaction, the E_a and E_c values are calculated in accord with departures from standard half-cell electrode potentials at unit activity because of the concentration changes by the Nernst Equation for a general half-cell reaction, given as [34, 37];

$$aA + mH^+ + ze^- \rightarrow bB + dH_2O \tag{2.5}$$

$$E = E^0 - \frac{RT}{zF} \ln \frac{(B)^b (H_2O)^d}{(A)^a (H^+)^m} \tag{2.6}$$

2.2 Electrochemical Kinetics of Corrosion

Kinetics of the electrochemical reaction is fundamental in the determination of the corrosion rate of a metal subjected to a corrosive medium that is electrolyte; on the contrary, although corrosion probability is predicted by thermodynamics, it does not give any information on the ways of occurrence of slow or fast corrosion. Since the reaction kinetics on an electrode surface is dependent on the electrode potential, the rate of electron flow to or from a metal-electrolyte interface determines the reaction rate. If the electrochemical system is at equilibrium then the net rate of reaction is equal to zero. Chemical kinetics controls reaction rates whereas electrochemical kinetics mainly controls corrosion rates [38].

2.2.1 Faraday's Law

The rate of electron flow to or from a reacting interface is a measure of reaction rate. The proportionality between current, *I*, in amperes, and mass reacted, *m*, in an electrochemical reaction is given by Faraday's Law [34];

$$m = \frac{ItA}{zF} \tag{2.7}$$

where *A* the atomic weight, and *t* the time. Dividing equation (2.7) through by *t* and the surface area, *a*, yields the corrosion rate, [34]; *r*

$$r = \frac{m}{ta} = \frac{iA}{zF} \tag{2.8}$$

where *i*, defined as current density (*I*/*a*). This equation gives the proportionality between mass loss per unit area per unit time (e.g., mg/dm^2/day) and current density (e.g., μA/cm^2). Units of penetration per unit time stem from dividing equation (2.8) by the density, *D*, of the alloy. For corrosion rate in millimeter per year, equation (2.8) becomes

$$r = C\frac{iA}{zD} \tag{2.9}$$

The proportionality constant, *C*, which includes *F* and any other conversion factor for units, for instance, *C* = 0.129 when corrosion rate is in mils per year, mpy, 0.00327 when units are in mm/year [39].

2.2.2 Energy Distribution

The only difference between the forward (ΔG_f) and reverse (ΔG_r) reactions is the change in activation energy for each reaction. Energies of them are shown in Figure 2.1 that is obeys distribution law of Boltzmann or Maxwell-Boltzmann for the energy distribution of

reversible electrodes of the reacting species (ions). If an overpotential polarized them by under steady-state conditions, the reactions rate is not equal, $Rf \neq Rr$ [38].

Commonly, reaction rates of the electrochemical and chemical resulted from either overpotentials of anodic or cathodic can be anticipated by using both Faraday and Arrhenius equations, respectively as depicted below:

$$R_F = \frac{iA_j}{zF} \tag{2.10}$$

$$R_A = \gamma_a \exp\left(-\frac{\Delta G^*}{RT}\right) \tag{2.11}$$

where i is the applied current density $\left(\frac{A}{cm^2}\right)$, whereas A_j is the atomic weight of species j (g/mol),

$A_{alloy} = \Sigma\ f_j \frac{A_j}{z_j}$ in units of g/mol, z_j and f_j are the valence number and weight fraction of element j, γ_a is the constant of chemical, ΔG^* is the activation energy of free energy change (j/mol) [38].

At equilibrium, rate equations of Faraday and Arrhenius become equal ($R_F = R_A$) and as a result, the current density becomes:

$$i = \gamma_0 \exp\left(-\frac{\Delta G^*}{RT}\right) \tag{2.12}$$

For a reversible electrode at equilibrium, the current density in equation (2.12) turns out the exchange current density; that is, $i = i_0$ [38].

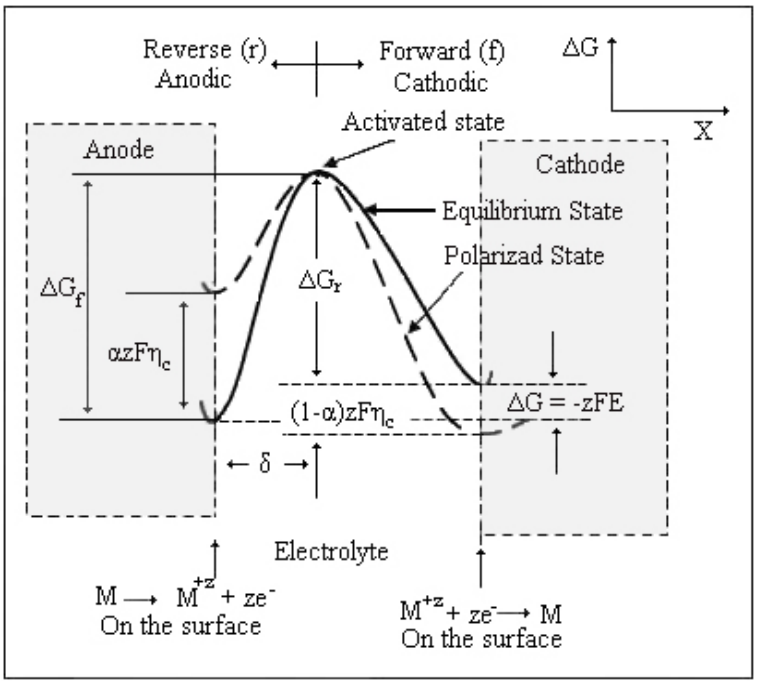

Figure 2.1 Schematic activation of free energy distribution [38].

On the other hand, when an overpotential polarized an electrode under steady-state conditions, the reactions rates are not equal ($R_F \neq R_A$) and therefore, the forward (cathodic) and reverse (anodic) current density must be described in terms of free energy change, ΔG^*, obtained from Figure 2.1 [38]. Therefore,

$$i_f = k_f^{'} \exp\left[-\frac{\Delta G_f^*}{RT}\right] \qquad \textit{Cathodic} \qquad (2.13)$$

$$i_r = k_r^{'} \exp\left[-\frac{\Delta G_r^*}{RT}\right] \qquad \textit{Anodic} \qquad (2.14)$$

where, $\Delta G_f^* = \Delta G_f - \alpha zF\eta_C$, $\Delta G_r^* = \Delta G_r + (1-\alpha)zF\eta_C$, α is symmetry coefficient [38]. Where, η_c is the cathodic overpotential, η_a is the anodic overpotential and *F* is the Faraday's constant.

For the cathodic reaction, the net current and the overpotential are $i = i_f - i_r$ and η_c, respectively. Substituting the equations (2.13) and (2.14) into this expression gives the net current density in a common form given by,

$$i = k_f^{'} \exp\left(-\frac{\Delta G_f}{RT}\right)\exp\left(\frac{\alpha z F \eta_c}{RT}\right) - k_r^{'} \exp\left(-\frac{\Delta G_r}{RT}\right)\exp\left[-\frac{(1-\alpha) z F \eta_c}{RT}\right] \qquad (2.15)$$

The exchange current density is defined as

$$i_0 = k_f^{'} \exp\left(-\frac{\Delta G_f}{RT}\right) = k_r^{'} \exp\left(-\frac{\Delta G_r}{RT}\right) \qquad (2.16)$$

By substituting equation (2.16) into (2.15) for one-step reaction we obtain the well-known Butler-Volmer equation (2.17) to polarize an electrode from the open circuit potential E_0 under steady-state conditions [38], where $\eta = E - E_0$:

$$i = i_0 \left\{ \exp\left[\frac{\alpha z F \eta_c}{RT}\right]_f - \exp\left[-\frac{(1-\alpha) z F \eta_c}{RT}\right]_r \right\} \qquad (2.17)$$

2.3 Electrochemical Polarization

The task of the electrode reactions is assumed to be the introduction of deviations from equilibrium caused by the passage of an electrical current through an electrochemical cell causing a change in the working electrode potential. This electrochemical fact is referred to as polarization. In the polarization process, the deviation from equilibrium results in an electrical potential difference between the polarized and the unpolarized electrode potential as over potential (η) [38].

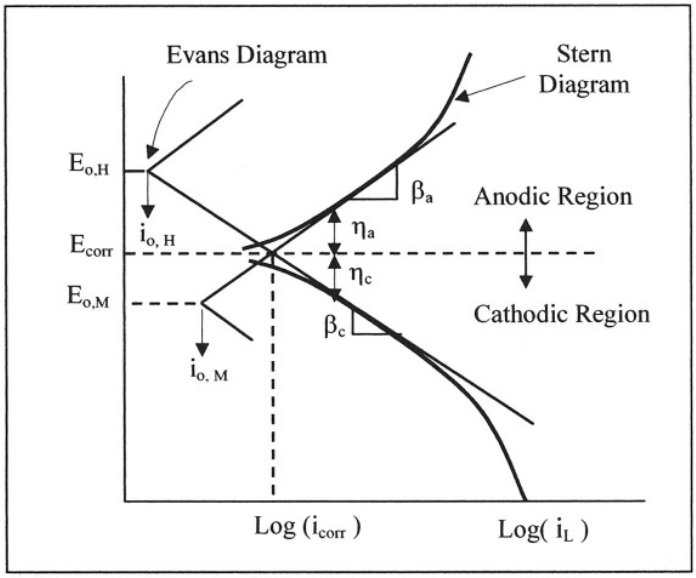

Figure 2.2 Schematic polarization curve showing Tafel extrapolation [38].

From Figure 2.2, $E_{0,H}$ and $E_{0,M}$ are the open-circuit potentials of hydrogen and metal, respectively, $i_{0,H}$, $i_{0,M}$ are the exchange current densities, i_L is the limiting current density [38].

For a reversible electrode, Evans diagram makes it possible to determine the corrosion point that is the interception point of the anodic and cathodic line; on the contrary, stern diagram of cathodic and anodic indicated the irreversible electrochemical behavior which is also useful for the determination of the corrosion point by simple extrapolation of the linear parts of both curves till the interception, as illustrated in Figure 2.2 [38].

The corrosion behavior is usually evaluated by using a function depending on kinetic parameters shown in Figure 2.2. Hence, the current density function for polarizing an electrode irreversibly from the corrosion potential is analogous to equation (2.17) [38]. Thus,

$$i = i_{corr}\left\{\exp\left[\frac{\alpha zF\eta}{RT}\right]_f - \exp\left[-\frac{(1-\alpha)zF\eta}{RT}\right]_r\right\} \tag{2.18}$$

Where, $\eta = E - E_{corr}$, E = applied potential (V).

2.3.1 Activation Polarization

Activation polarization is essentially an electrochemical fact pertained to a charge-transfer mechanism, in which the rate of electron flow from a metal surface experiencing oxidation is controlled by a particular reaction step. Rate of the electron flow is controlled by the slowest step in the half-cell reactions [38].

In general, the anodic metal experiences successive reaction steps before dissolution in the electrolyte. This successary is theoretically represented by the following idealized reactions of oxidation of metal occurring in the activation polarization session.

$$M_{lattice} \rightarrow M^{+z}_{surface} \rightarrow M^{+z}_{solution} \tag{2.19}$$

For hydrogen evolution, in order to describe the reaction steps in succession which might occur after hydrogen cations are adsorbed on the electrode surface, idealized model of Fontana [38] for activation polarization shown in Figure 2.3 is useful. Hence, the possible reactions are:

$$H^+ + e^- \rightarrow H \qquad \textit{Atomic hydrogen} \tag{2.20}$$

$$H + H \rightarrow H_2 \qquad \textit{Hydrogen molecule} \tag{2.21}$$

$$H_2 + H_2 \rightarrow 2H_2 \qquad \textit{Gas bubble} \tag{2.22}$$

Thus, only one step equation (2.19) and one in equation (2.20) and (2.21) controls the charge transfer for activation polarization [38].

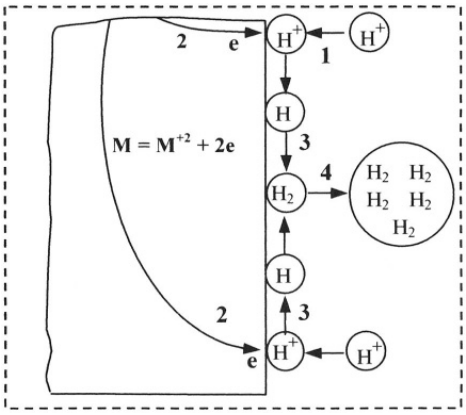

Figure 2.3 Activation polarization model [38].

2.3.2 Concentration Polarization

As the potential of an electrode is changed far away from its equilibrium potential, the net current flowing, whether anodic, (i_a), or cathodic, (i_c), increases at first according to the Tafel equation (2.23). However, the current cannot be increased for a long time since there are limits to the rate at which ions can carry charges through the solution to and from the electrode. This results in an excess potential over that predicted by the Tafel equation. The situation is illustrated in Figure 2.4 [39].

$$\eta = \beta \log\left(\frac{i}{i_0}\right) \tag{2.23}$$

where, η is the overpotential (*V*), β is the tafel slope (*V*), i is the applied current density $\left(\frac{A}{cm^2}\right)$, i_0 is the exchange current density $\left(\frac{A}{cm^2}\right)$.

The effect occurs because ions are produced or consumed at the electrode surface faster than they can diffuse to or from the solution bulk. In an anodic reaction, the concentration of ions in the immediate vicinity of the electrode is increased above that in the bulk solution; unlike, in a cathodic reaction, the local concentration is depressed. In conclusion, the

polarization for a given current is greater than that predicted by the Tafel equation. The excess potential is called the concentration polarization, η_c [39].

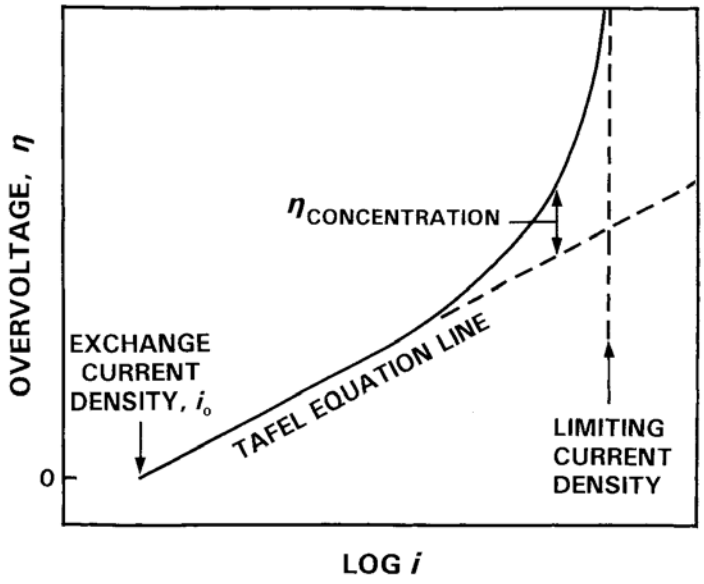

Figure 2.4 Logarithmic plot of current density, *i*, vs. overvoltage, η for a polarized electrode, showing deviation from Tafel line and limiting current density because of concentration polarization. η is positive for an anodic current and negative for a cathodic current [39].

2.4 Passivity

A metal is considered passive if it is converted to a stable oxide, since that oxide constitutes a barrier between the metal and its environment. The corrosion is either eliminated or retarded when a surface film of an oxide or hydroxide develops. The thickness of the passive films might be as small as 2-10 nm. These films offer a limited electronic conductivity and behave similar to semiconductors with metallic properties rather than the properties of bulk oxides. The films also permit a limited amount of conductivity of cations due to the lattice defects and a slow anodic dissolution. However, a reduction in the cathodic polarization current density and an increase in the anodic polarization current density are resulted from the film formation. Furthermore, retardation of corrosion is stemmed from the above factors. But the most important point is that once a film is formed the corrosion rate decreases sharply. The

anodic dissolution process is inhibited by the passivity on the metal surface that develops due to film formation [40].

Such metals are referred as active-passive metals. The most basic characteristic of these metals is S-shaped polarization curves. The anodic dissolution behavior of a metal exhibited an active-passive behavior as illustrated in Figure 2.5. The reversible potential of a hypothetical metal M is indicated by $E_{(M/M^{Z+})}$, oxygen by $E_{rev}(O)$. The anodic and cathodic polarization curves in the active region intersect at the corrosion potential, (E_{corr}). The anodic curve displays a Tafel behavior with a slope β_a, whereas the cathodic curve can be obtained by deviation from E_{corr} in the active direction and the cathodic Tafel slope is given by β_c and the intersection point gives E_{corr}. While polarizing the metal in the noble direction from E_{corr}, it is possible to see the rate of metal dissolution raises as the potential raieses. The highest corrosion rate is achieved at a maximum current density, referred as critical current density ($i_{critical}$). In the lower portion of the anodic curve (nose of the curve), it is possible to see a Tafel relationship up to $i_{critical}$ that is the amount of current required for the generation of high concentration of metal cations so that the nucleation and growth of the surface firm can proceed. The potential corresponding to $i_{critical}$ is called the primary passive potential (E_{pp}) as it represents the transition of a metal from an active state to a passive state. Due to the onset of passivity, the current density (*log i*) tends to decrease beyond E_{pp}, resulting from the oxide film formation on the metal surface. Beyond E_{pp}, the current keeps on decreasing until it reaches a certain potential value and finally it drops to a value that is orders of magnitude lower than $i_{critical}$. Furthermore, the lowest current density needed for the maintaining process of the metal in a passive state is called passive current density (i_p), which is an intrinsic property of oxidation. At i_p, the metal dissolution occurs at a constant rate and the oxide film starts to get thicker [40].

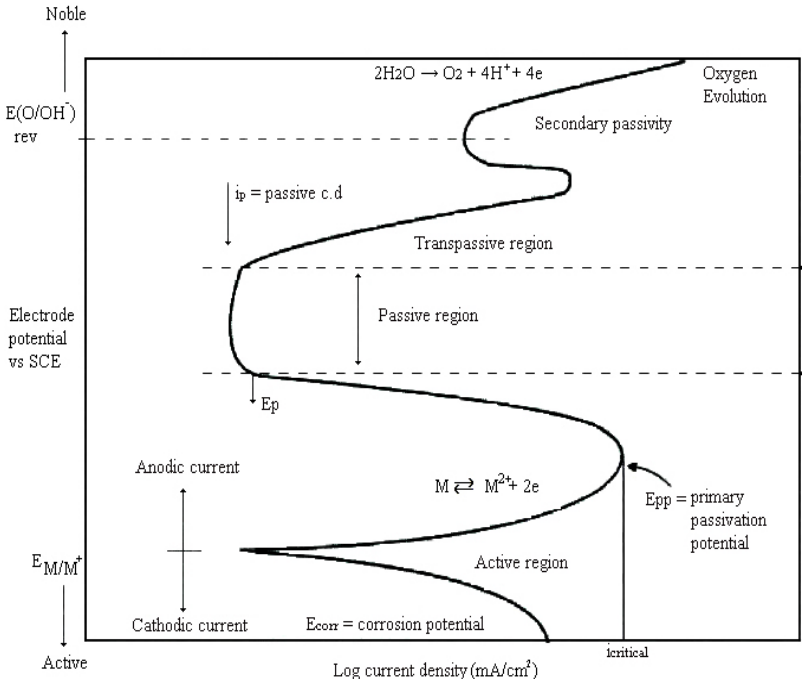

Figure 2.5 Anodic dissolution behavior of a metal [40].

2.5 Polarization Methods

2.5.1 Linear Polarization

Using equation (2.18) under anodic and cathodic polarization individually, the Tafel slopes are derived by letting $\exp\left[\frac{\alpha zF\eta_a}{RT}\right]_f >> \exp\left[-\frac{(1-\alpha)zF\eta_a}{RT}\right]_r$ for an anodic polarization analysis, where $i_a >> |i_c|$ and $\eta_a >> \eta_c$. On the other hand, $\exp\left[\frac{\alpha zF\eta_c}{RT}\right]_f << \exp\left[-\frac{(1-\alpha)zF\eta_c}{RT}\right]_r$ is for characterizing cathodic polarization when $|i_c| >> i_a$ and $\eta_c >> \eta_a$. Under these conditions, equation (2.17) reduces to

$$i_a = i_0 \exp\left[\frac{\alpha zF\eta_a}{RT}\right] \qquad (\text{for } i_a >> i_c,\ \eta_a >> \eta_c) \qquad (2.24)$$

$$i_c = -i_0 \exp\left[\frac{(1-\alpha)zF\eta_C}{RT}\right] \quad (\text{for } i_c >> i_a,\ \eta_c >> \eta_a) \tag{2.25}$$

solving equations (2.24) and (2.25) for the overpotentials yields

$$\eta_a = \beta_a \log\left(\frac{i_a}{i_o}\right) \tag{2.26}$$

$$\eta_c = -\beta_c \log\left(\frac{i_c}{i_o}\right) \tag{2.27}$$

where β_a and β_c are corresponded as Tafel slopes of the anodic and cathodic reactions, respectively. These slopes are defscribed by

$$\beta_a = \frac{2.303RT}{\alpha zF} = \frac{(1-\alpha)\beta_c}{\alpha} \tag{2.28}$$

$$\beta_c = \frac{2.303RT}{(1-\alpha)zF} = \frac{\alpha\beta_a}{(1-\alpha)} \tag{2.29}$$

Figure 2.6 illustrates hypothetical polarization curves of polarization resistance [38].

Before determining i_{corr}, the polarization resistance R_p is anticipated from the linear slope of the curve as

$$R_p = \frac{\Delta E}{\Delta i} = \frac{\eta}{\Delta i} \tag{2.30}$$

where the corrosion current density, i_{corr}, depends on this parameter in a later derived functional form.

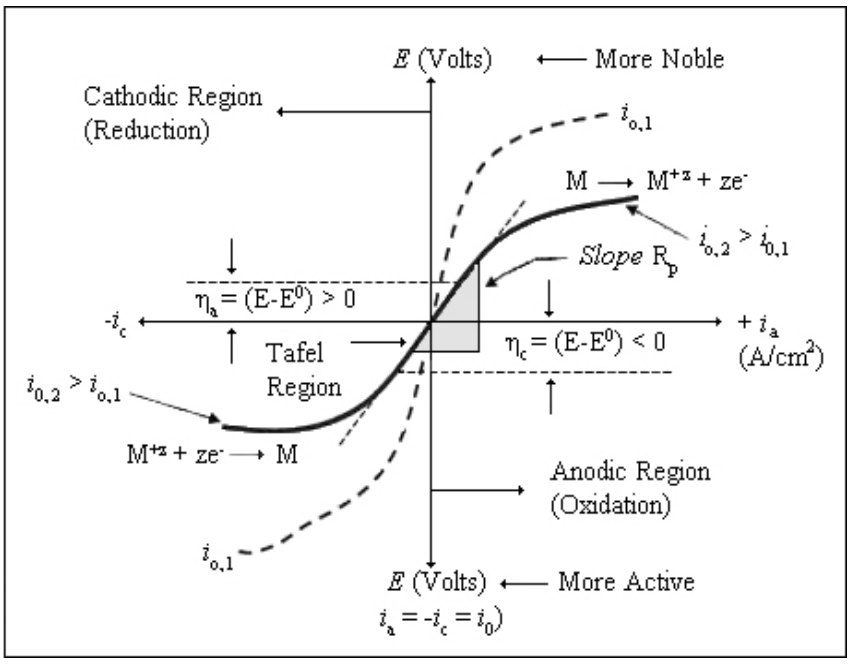

Figure 2.6 Curve of schematic linear polarization [33].

2.5.2 Tafel Extrapolation

In the Tafel Extrapolation method, the Tafel slopes β_a and β_c as well as E_{corr} and i_{corr} from a single polarization curve as depicted in Figure 2.2 is determined. This curve is also called the Stern diagram, non-linear polarization, based on equation (2.18). The Evans diagram, linear polarization, is also involved so as to make sure that both diagrams have a common $E_{corr} \cdot i_{corr}$ point. This figure shows a theoretical electrochemical behavior of a metal immersed in an electrolyte [38].

Determination of the corrosion point of electrochemical systems containing several oxidizers is more complex by Evans diagram than the Stern diagram which would provide a polarization curve similar to the one depicted in Figure 2.2 from which both E_{corr} and i_{corr} are determined by simply extrapolating the linear parts of the Tafel anodic and cathodic till their intersection becomes a straight line. Moreover, depicted in Figure 2.2 are the exchange current densities, $i_{0,H}$ and $i_{0,M}$, and their counterpart potentials, $E_{0,H}$ and $E_{0,M}$, for evolution of hydrogen and oxidation of metal, respectively. $E_{0,H}$ and $E_{0,M}$ are known as open-circuit

potentials. In addition, the limiting current density (i_L) for cathodic polarization is included as additional information that one can extract from a cathodic polarization curve [38].

2.5.3 Corrosion Rate

Throughout corrosion (oxidation) process, anodic and cathodic reaction rates are matched together on the electrode surface at a specific current density shown as $i_{corr.}$ This is an electrochemical phenomenon in which the occurance of both reactions on different sites on the metal/electrolyte interface is necessary. For a uniform process under steady state conditions, the relation of the current densities at equilibrium is $i_a = -i_c = i_{corr}$ at E_{corr} assuming that the corrosion is uniformed and the oxide film formed on the metal electrode surface is not seen; otherwise things would get complex. The goal at this point is to determine both E_{corr} and i_{corr} either using the Tafel Extrapolation or Linear Polarization methods. It is prominent to indicate that i_{corr} cannot be measured at E_{corr} since $i_a = -i_c$ and current do not flow through an external device of current-measuring [38].

As polarizing from the corrosion potential with respect to anodic or cathodic current density, the overpotential expressions given by equations (2.26) and (2.27) become

$$\eta_a = \beta_a \log\left(\frac{i_a}{i_{corr}}\right) \tag{2.31}$$

$$\eta_c = -\beta_c \log\left(\frac{i_c}{i_{corr}}\right) \tag{2.32}$$

Recall that $\eta_a = \Delta E = (E - E_{corr}) > 0$ and $\eta_a = \Delta E = (E - E_{corr}) < 0$ now show the potential changes from the steady-state corrosion potential E_{corr} [38]. Solving equations (2.31) and (2.32) for the anodic and cathodic current densities yield, respectively

$$i_a = i_{corr} \exp\left[\frac{2.303(E - E_{corr})}{\beta_a}\right] \tag{2.33}$$

$$i_c = i_{corr} \exp\left[-\frac{2.303(E - E_{corr})}{\beta_c}\right] \tag{2.34}$$

Assuming that the applied current density is $i = i_a - i_c$ and substituting equations (2.33) and (2.34) into this expression gives the Butler-Volmer equation that evaluates the electrochemical corrosion kinetics.

$$i = i_{corr}\left\{\exp\left[\frac{2.303(E - E_{corr})}{\beta_a}\right] - \exp\left[-\frac{2.303(E - E_{corr})}{\beta_c}\right]\right\} \tag{2.35}$$

This expression resembles equation (2.18); however, it is a proper expression at that point because the inverse polarization resistance is easily achievable by deriving equation (2.35) with respect to the applied potential *E* [38]. Therefore,

$$\left(\frac{di}{dE}\right) = 2.303 i_{corr}\left\{\beta_a^{-1} \exp\left[\frac{2.303(E - E_{corr})}{\beta_a}\right] - \beta_c^{-1} \exp\left[\frac{-2.303(E - E_{corr})}{\beta_c}\right]\right\} \tag{2.36}$$

Further,

$$\left(\frac{d^2 i}{dE^2}\right) = 5.3038 i_{corr}\left\{\beta_a^{-2} \exp\left[\frac{2.303(E - E_{corr})}{\beta_a}\right] - \beta_c^{-2} \exp\left[\frac{-2.303(E - E_{corr})}{\beta_c}\right]\right\} \tag{2.37}$$

Let's set some conditions for equation such that

$$\left(\frac{d^2 i}{dE^2}\right) \Rightarrow \left\{\begin{array}{c} < 0 \text{ for } E = E_{\max} > E_{corr} \\ = 0 \text{ for an inflation point: } E = E_{corr} \\ > 0 \text{ for } E = E_{\max} < E_{corr} \end{array}\right\} \tag{2.38}$$

Evaluating equation (2.37) at the inflation point yields

$$\left(\frac{d^2 i}{dE^2}\right)_{E=E_{corr}} = 5.3038 i_{corr}\left(\beta_a^{-2} - \beta_c^{-2}\right) \tag{2.39}$$

which shows that the inflection point is accomplished if and only if $\beta_a = \beta_c$ [6]. This condition was indicated by Oldham and Mansfield [41] as the mathematical proof of $E_{corr} \cdot i_{corr}$ point shown in Figure 2.2.

Also, evaluating equation (2.36) at $E = E_{corr}$ gives the polarization resistance

$$\frac{1}{R_p} = \left(\frac{di}{dE}\right)_{E=E_{corr}} = 2.303 i_{corr}\left(\frac{\beta_a + \beta_c}{\beta_a \beta_c}\right) \tag{2.40}$$

Thus, the functional form between R_p and i_{corr} have been obtained as

$$R_p = \frac{\beta_a \beta_c}{2.303 i_{corr}\left(\beta_a + \beta_c\right)} \tag{2.41}$$

Defining the Stern-Geary coefficient, B as

$$B = \frac{\beta_a \beta_c}{2.303\left(\beta_a + \beta_c\right)} \tag{2.42}$$

Corrosion current density is simply,

$$i_{corr} = \frac{B}{R_p} \tag{2.43}$$

Recalling Eqn. 2.10, corrosion rate will then be in mm/year,

$$r = 0.00327 \frac{i_{corr} A}{zD} \tag{2.44}$$

CHAPTER 3

EXPERIMENTAL DETAILS

3.1 Specimen Preparation

In this study five binary, three ternary and two quaternary alloys were made by induction melting and casting. The selected elements were Bi, Cd, Mg and Sn. For reference point of view, pure Pb and Pb-Sb binary alloy specimens were also made, since Sb is a common alloying element in battery grids. The binary phase diagrams are given in Figure 1.3 to 1.7. As can be seen in these diagrams all alloying elements have limited solid solubility in Pb and only in Pb-Mg and Pb-Bi system there is an intermetallic compound that is stable at room temperature (RT).

Pure metals in desired amounts were put in a graphite crucible and melted under atmospheric conditions. The liquid alloy was then poured into a pre-heated graphite mould having a 60x100x5 mm cavity. The chemical composition of the alloys was determined by optical emission spectroscopy and is given in Table 3.1.

The slabs were then rolled at RT to reduce their thickness to 3 mm, from which circular specimens having approximately 20 mm diameter were cut. Copper cables were soldered on one side of the samples, which were then embedded in polyester resin having the other side of the sample to be exposed to the corrosion medium.

All specimens were ground by 120 to 1200 grit emery paper and also chemically polished with a solution of 75 ml acetic acid (CH_3COOH) + 25 ml hydrogen peroxide (H_2O_2) for shiny appearance. Finally, specimen surfaces rinsed by water and then with alcohol and dried in fan air.

Table 3.1 The chemical composition of Pb alloys.

	Sn (wt. %)	Mg (wt. %)	Bi (wt. %)	Cd (wt. %)	Sb (wt. %)
Pb	-	-	-	-	-
Pb-Bi	-	-	0.19	-	-
Pb-Cd	-	-	-	0.21	-
Pb-Mg	-	0.013	-	-	-
Pb-Sb	-	-	-	-	1.59
Pb-Sn	1.57	-	-	-	-
Pb-Bi-Sn	1.61	-	0.19	-	-
Pb-Cd-Sn	1.53	-	-	0.17	-
Pb-Mg-Sn	1.55	0.011	-	-	-
Pb-Cd-Mg-Sn	1.52	0.011	-	0.20	-
Pb-Mg-Bi-Sn	1.46	0.012	0.18	-	-

The corrosion and gas evolution experiments were carried out in 3.75 M (1.23 sp. gr.) H_2SO_4 solution at RT. The test solutions were prepared freshly with stirring and used not more than four times because of possible breakdown of solution purity.

The microstructural characterizations were made by NIKON Optiphot Microscope. The specimens were etched by 10 gr ammonium molybdate ($(NH_4)_6Mo_7O_{24}{\cdot}4H_2O$) + 10 gr citric acid ($C_6H_8O_7$) + 100 ml deionized water solution.

Hardness was measured at seven different sites of the specimens' surface by Shimadzu Micro Hardness Tester Machine with Vickers intender under constant load of 0.1 N.

3.2 Electrochemical Experiments

3.2.1 Open Circuit Potential (OCP) Measurement

The open circuit potential measurements were carried out in 3.75 M H_2SO_4 for 1 h using a counter electrode (Pt) and a saturated calomel reference electrode (SCE).

3.2.2 Anodic Polarization Measurement

The electrochemical polarization cell is a 1 L glass kit and a teflon lid with four openings for working and counter electrodes, thermometer, and a reference electrode. In this design, the specimen with a flat surface is positioned at one side of the flask facing the platinum counter electrode.

The potential of the working electrode is measured by means of reference electrode. This is achieved with using the lugging probe, which is flexibly mounted to the flask and probe tip was established near the specimen surface to diminished *IR*-drop which means voltage drop. The electrolyte is carried between the reference and working electrode by the salt bridge. The SCE is used as a reference electrode, which is positioned in a salt bridge SCE electrode is composed of Hg_2Cl_2, mercury and saturated potassium chloride solution and also platinum wire provides electrical connection into corrosion cell. The specimen, counter electrode and a calomel reference electrode are connected to Solartron 1480 Multi Channel potentiostat. The potentiostat is controlled by Corrware software, which allows the control of the test parameters to be specified and the results to be executed.

Potentiodynamic polarization measurements were done for passivated surface conditions. Before each experiment a cathodic polarization at a potential of -1.2 V for 10 min was applied with the intention of removing any oxidation products formed by aerial oxidation during pretreatments. Then the specimens were passivated for 1 h under open circuit condition, following passivation treatment, anodic scan has been started from -0.03 V vs open-circuit voltage (OCV) to 0 V vs reference electrode with the 0.3333 mV/s scan rate. Then, the potentiodynamic polarization curves were examined to determine primary passivation potential, E_{pp}, critical current density, $i_{critical}$, passive potential, E_p, passivation current density, i_p, transpassive potential, $E_{transpassive}$ and transpassive current density, $i_{transpassive}$, respectively.

3.2.3 Polarization Resistance Measurement

In order to determine the exact corrosion potential, E_{corr} and corrosion current density, i_{corr} and also corrosion rates of the specimens, polarization resistance technique was used.

Polarization resistance measurements were also carried out for the passivated samples. Similarly, a cathodic polarization at a potential of -1.2 V vs SCE for 10 min was performed. Initially, the specimens were held at open circuit condition for 1 h. To determine the corrosion rate, linear polarization experiment was perfomed from -0.03 V to + 0.03 V vs OCV with a scan rate of 0.1167 mV/s.

To calculate the corrosion potential, E_{corr}, corrosion current density, i_{corr}, and corrosion rates of the alloys, a computer program, fortran, has been written to process the experimental data. In this program, firstly, *I* vs *E* data was spline fitted in the range from ±10 mV around the corrosion potential, E_{corr}. Then, the root of the spline curve was calculated where the corresponding potential is the corrosion potential. After that, again with the same range, *I* vs *E* data this time was fitted to a line where the reciprocal of the slope gave the polarization resistance, R_p.

According to equation (2.40), if equation (2.41) that is Stern-Geary coefficient is known, corrosion potential can be evaluated from R_p. Hence, so as to calculate, B, the approach proposed by Mansfeld [42] was used. In this approach, I_{corr} in Butler-Volmer equation (2.17) was substituted by $\frac{B}{R_p}$, giving that;

$$I = \frac{B}{R_p}\left\{\exp\left(\frac{2.303(E-E_{corr})}{\beta_a}\right) - \exp\left(\frac{-2.303(E-E_{corr})}{\beta_c}\right)\right\} \qquad (3.1)$$

This equation was optimized, using principal axis minimization method, with respect to β_a and β_c for every point in the data set, so that, both sides of equation (3.1) agree with each other with a minimum error. After optimization the agreement was, generally found to be in the order of 10^{-7}. Therefore, using Tafel constants, B was evaluated and i_{corr} can be calculated by equation (2.17).

Consequently, the corrosion rates in mm/year was evaluated using;

$$C_R = \frac{0.00327(eqw)10^6 i_{corr}}{D} \quad (3.2)$$

where *eqw* is the equivalent weight in gr, 0.00327 comes from the unit conversion of time parameter, i_{corr} is corrosion current density and D is density in gr/cm^3.

3.2.4 Gas Evolution Measurement

In order to determine the hydrogen gas evolution that is to be experienced at the negative plate under charging conditions of the battery, the alloys were held at constant cathodic potentials during which liberated gas was collected and measured volumetrically.

Measurements were started at -0.4 V vs OCV. At this potential, liberated gas was collected for a period of 4500 sec. Then the potential was decreased by 0.1 V and gas collection continued for another 4500 sec. This stepwise decrease of the potential and gas collection was repeated three more times.

The glass kit which was used in this measurement has four openings; for working and counter electrodes, burette to measure volume of gas liberation and reference electrode salt bridge photograph of which is shown in Figure 3.1.

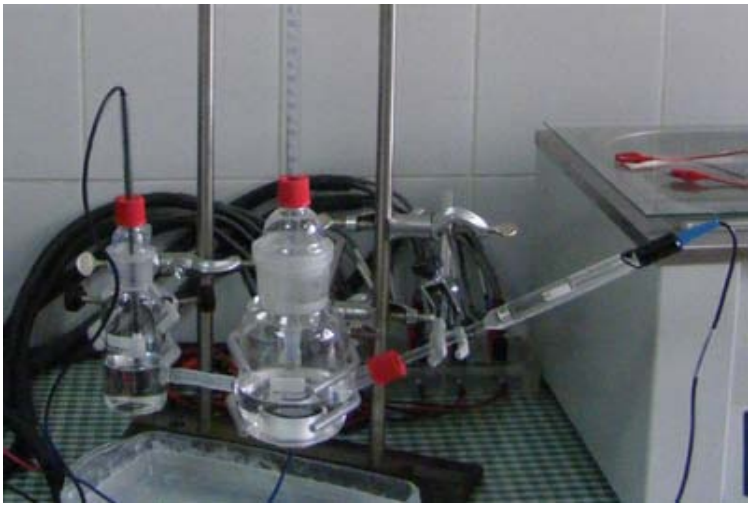

Figure 3.1 Photograph of the electrochemical glass kit used for gassing measurements.

3.2.5 PbO Conductivity Measurement

The conductivity of the passive film formed on the grid alloy was evaluated with an electrochemical procedure as outlined by Albert [20] and Miraglio [21]. In this procedure, anodized samples were scanned from + 0.2 V to – 1.2 V at a sweep rate of 1 mV/s, three times consecutively. During the first scan, the oxidation current of water at 1.4 V and the amount of PbO_2 reduced to $PbSO_4$ (measured by the corresponding peak area) depended closely on the conductivity of the PbO layer. All the Pb contained in the corrosion product was turned into metallic form at the end of the first cycle. Thus, during the next scan, both the current of oxidation of water and the peak area associated with the reduction of PbO_2 to $PbSO_4$ increase. Scans 2 and 3 resulted in voltammograms that are very similar.

Two passivation criteria have been investigated. These are denoted by *R* and *C*. Namely: *R* is the intensity ratio of the water oxidation peak according to:

$$R = \frac{I_3(mA)\text{for the third scan at 1400mV}}{I_1(mA)\text{for the first scan at 1400mV}}$$

and C is the peak area (P) ratio corresponding to PbO_2 reduction to $PbSO_4$ given by.

$$C = \frac{P_3 \text{ for the third scan}}{P_1 \text{ for the first scan}}$$

Consequently, when *R* and *C* values are close to 1, the corrosion layer, mainly constituting of PbO, is supposed to be more conductive, and the passivation is suppressed [21].

CHAPTER 4

RESULTS AND DISCUSSION

4.1 Microstructural Examinations

Optical micrographs of the specimens are given in Figures 4.1 to 4.11. The average grain size in Pb-Mg, Pb-Mg-Bi-Sn alloys is approximately 50 µm wheras it is about 30 µm in Pb-Cd, Pb-Mg-Sn, Pb-Cd-Mg-Sn alloys are. The grain size of Pb, Pb-Bi, Pb-Sb, Pb-Sn, Pb-Bi-Sn and Pb-Cd-Sn alloys is in the range of 100 to 400 µm.

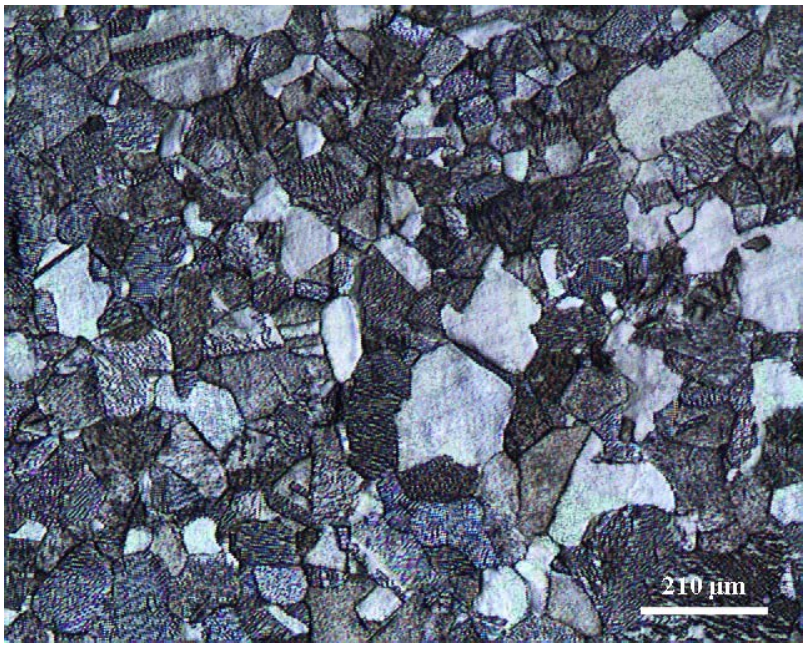

Figure 4.1 Microstructure of Pure Pb. Magnification: 50x.

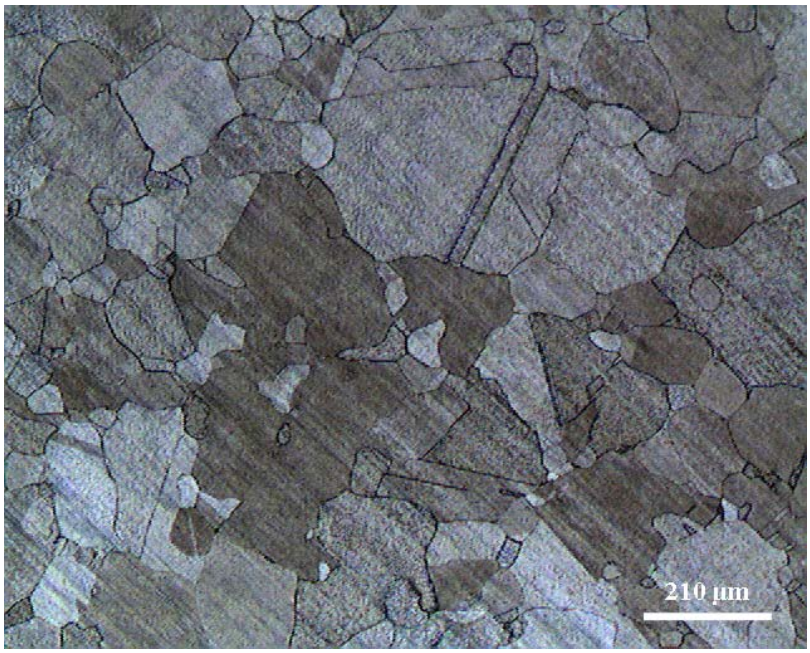

Figure 4.2 Microstructure of Pb-Bi. Magnification: 50x.

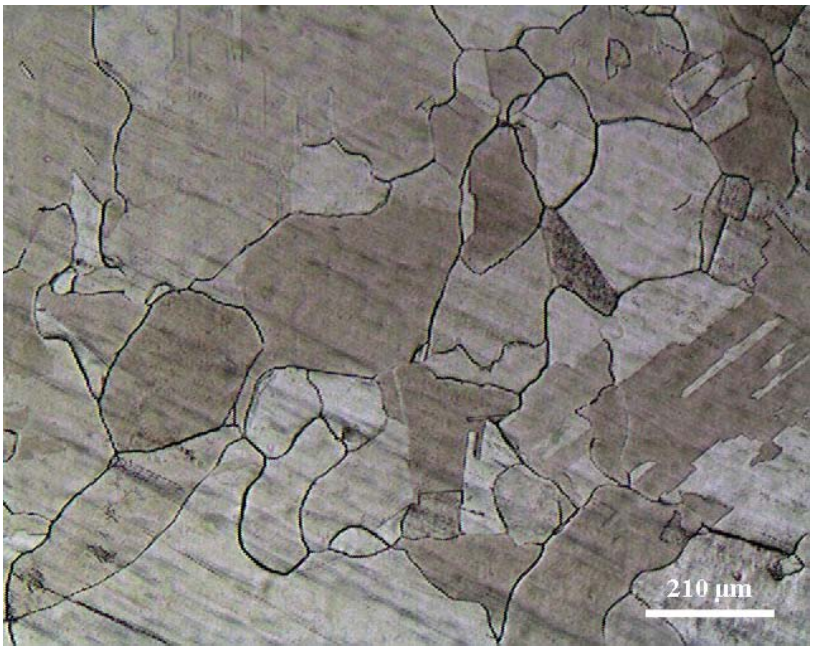

Figure 4.3 Microstructure of Pb-Cd. Magnification: 50x.

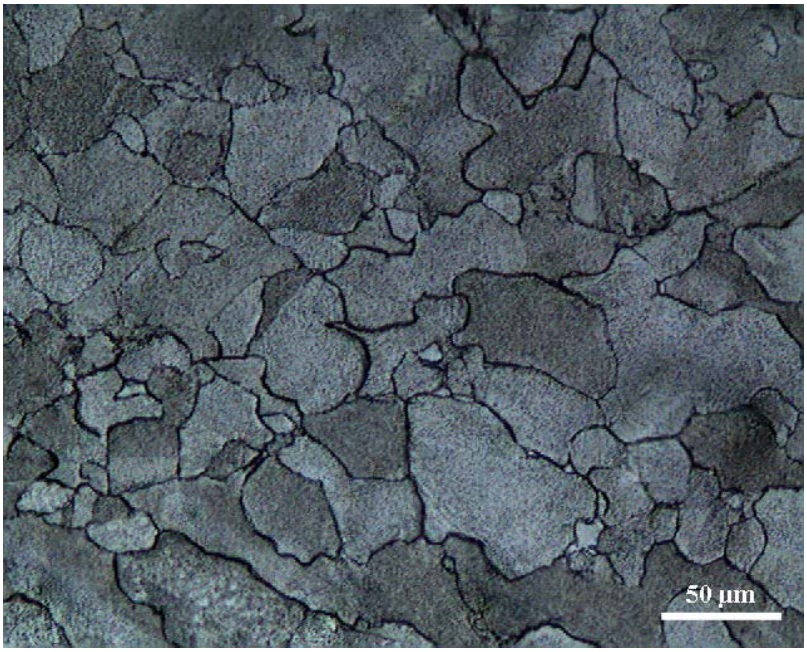

Figure 4.4 Microstructure of Pb-Mg. Magnification: 200x.

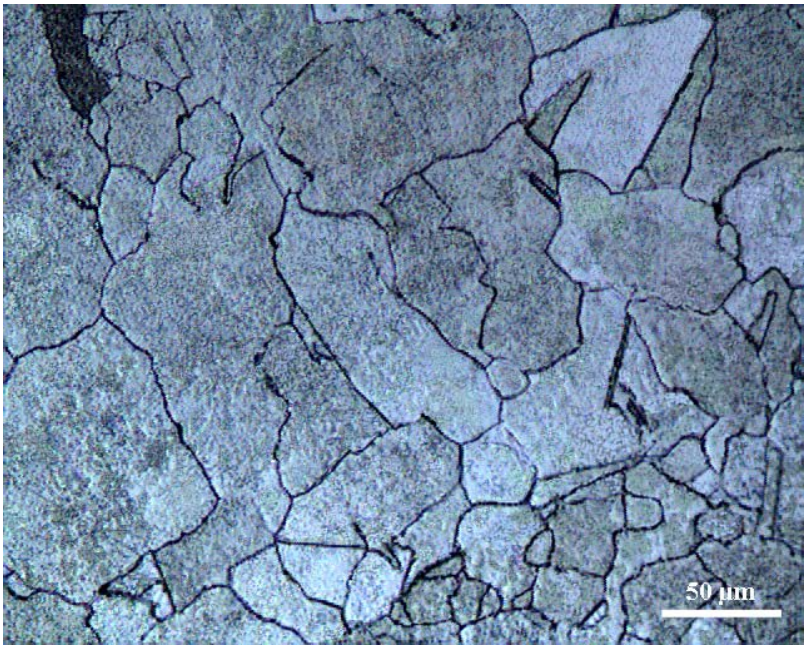

Figure 4.5 Microstructure of Pb-Sb. Magnification: 200x.

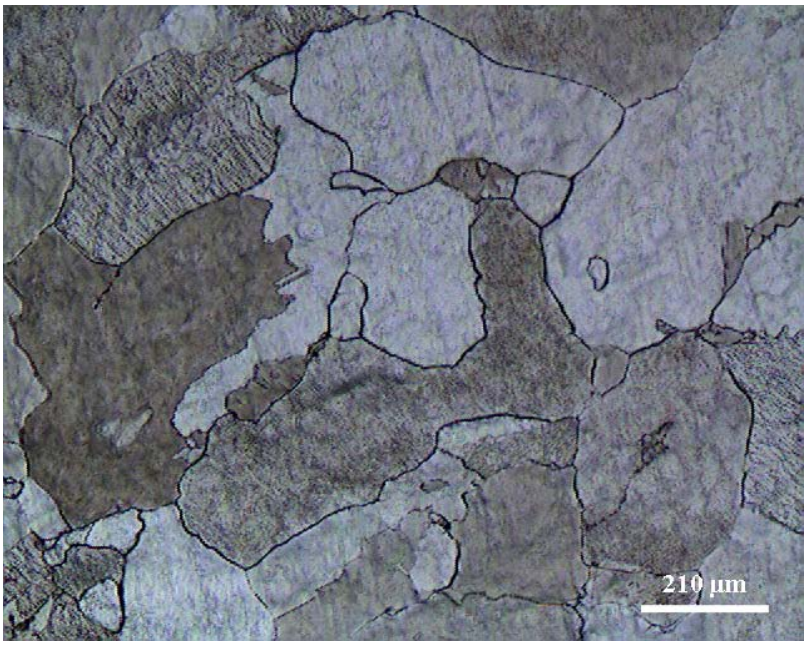

Figure 4.6 Microstructure of Pb-Sn. Magnification: 50x.

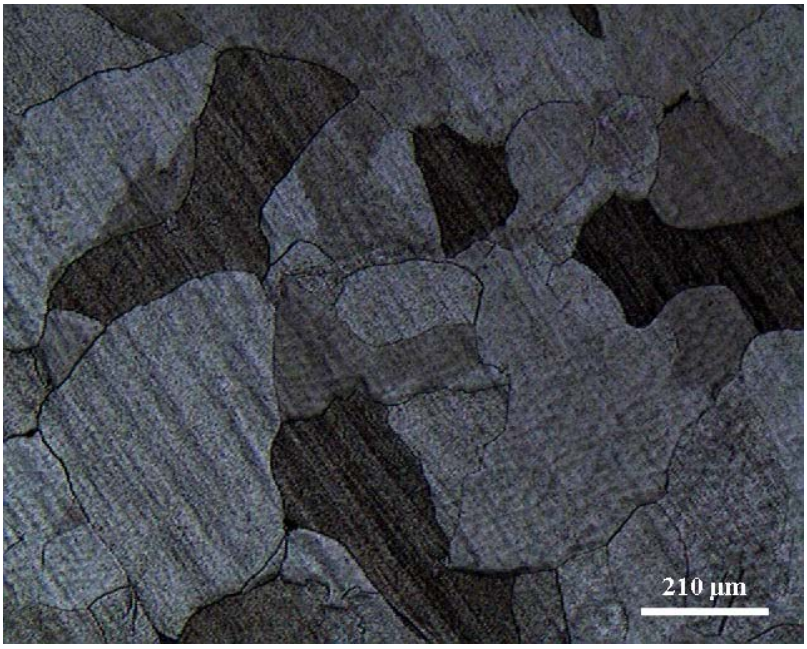

Figure 4.7 Microstructure of Pb-Bi-Sn. Magnification: 50x.

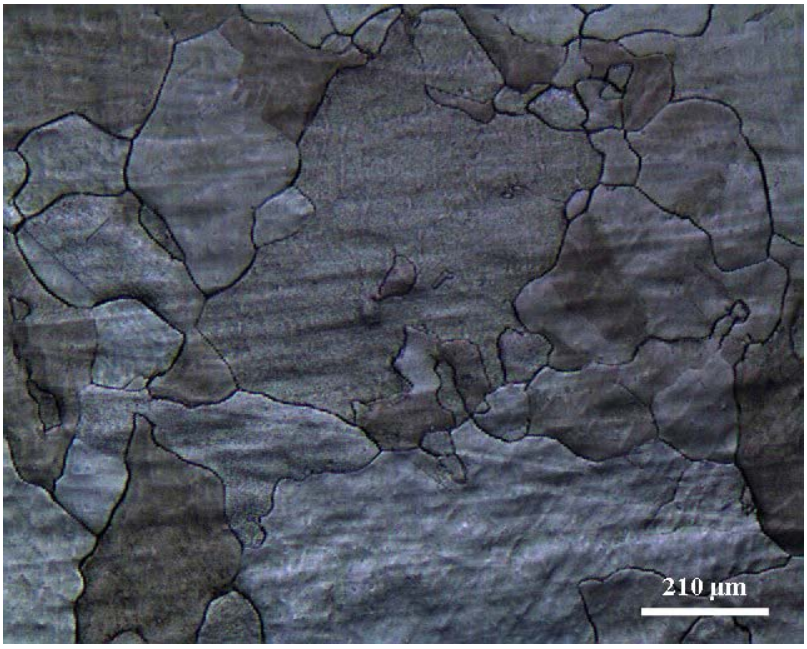

Figure 4.8 Microstructure of Pb-Cd-Sn. Magnification: 50x.

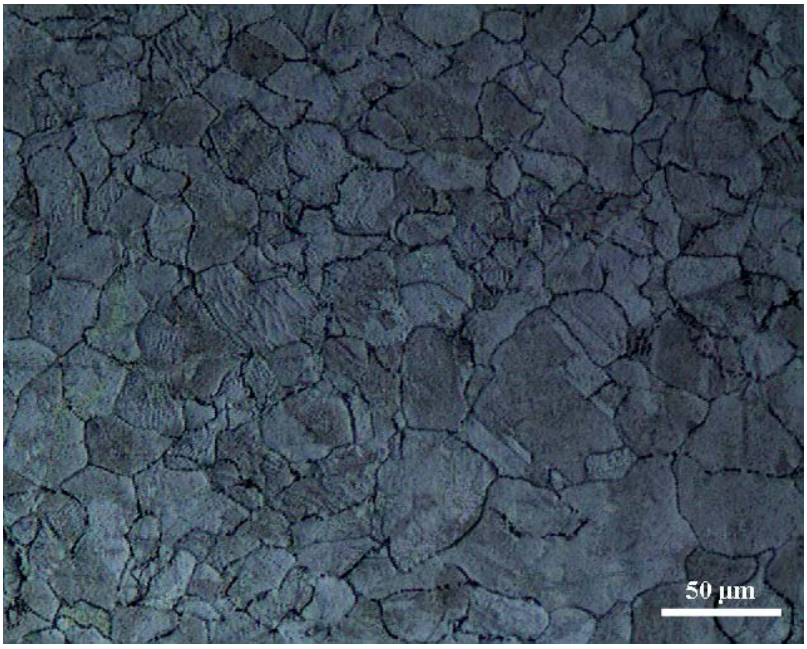

Figure 4.9 Microstructure of Pb-Mg-Sn. Magnification: 200x.

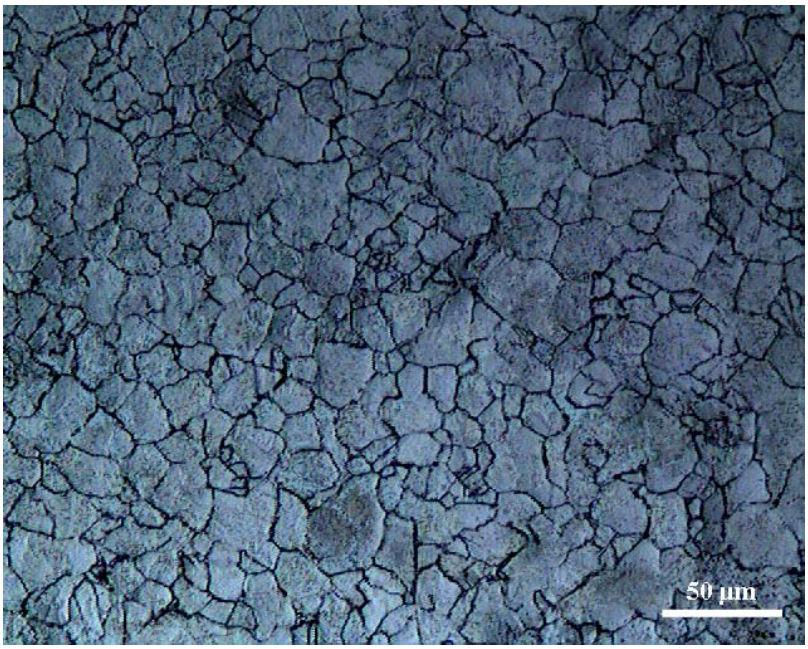

Figure 4.10 Microstructure of Pb-Cd-Mg-Sn. Magnification: 200x.

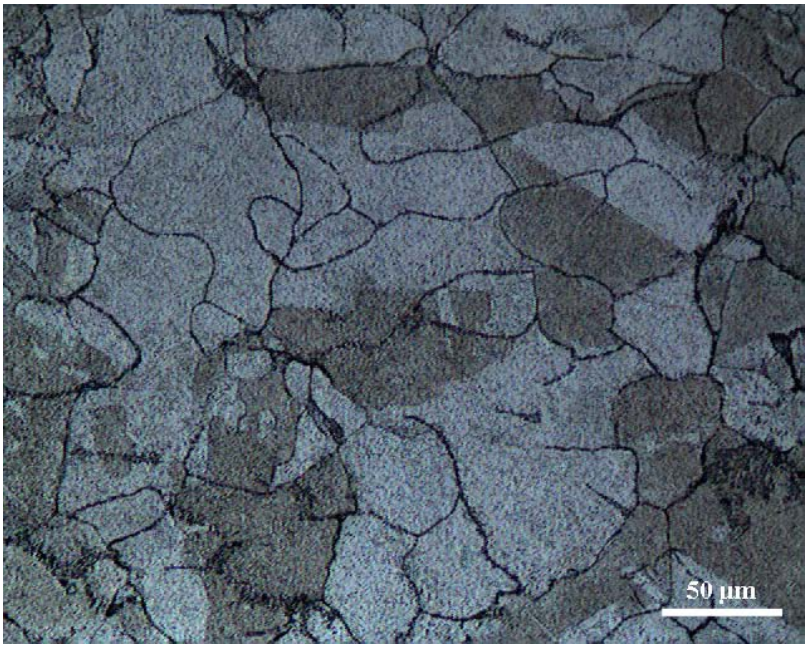

Figure 4.11 Microstructure of Pb-Mg-Bi-Sn. Magnification: 200x.

4.2 Hardness Measurements

It is obvious that pure Pb is too soft to be used as a grid material, so it has to be hardened somehow [8]. The effect of the added alloying elements on the hardness of the alloys can be seen in Figure 4.12 in which alloys were ordered with respect to their corrosion rate.

The minimum hardness values were obtained in Pb and Pb-Bi alloy. It can be seen from the phase diagram of Pb-Bi that the alloy is in solid solution and the mismatch between the metallic radii of the elements is less than 3 %. The fact that Pb-Bi alloy had the smallest hardness value close to that of Pb may be because of this. As can be seen Mg containing alloys have the highest hardness values amongst all. The reason for this may be because of the possible presence of intermetallic compound, Mg_2Pb and other probable intermetallics. Besides, higher tendency of Mg to oxidation compared to other metals increases the possibility of oxide layer occurence which may also increase the hardness value. Local strain-hardening, creates harder surface region is caused by this oxide layer [43]. Pb-Cd, Pb-Sb and Pb-Sn alloys have average hardness values. In ternary alloy systems, the results that were obtained from this study in which Sn was added to the binary alloys are as follows: The addition of Sn to Pb-Bi alloy resulted in the increase of the hardness value compared to Pb-Bi alloy. Addition of Sn to Pb-Cd system did not have much effect on the hardness value. In case of the addition of Sn to Pb-Mg alloy, hardness increases. In Pb-Mg-Sn two different kinds of intermetallic compounds, namely Mg_2Sn and Mg_2Pb may be formed according to Pb-Mg-Sn phase diagram. Addition of Bi and Cd to Pb-Mg-Sn ternary alloy system, the current hardness value was decreased a little. It can be also observed that the alloys having high hardness have generally smaller grain size.

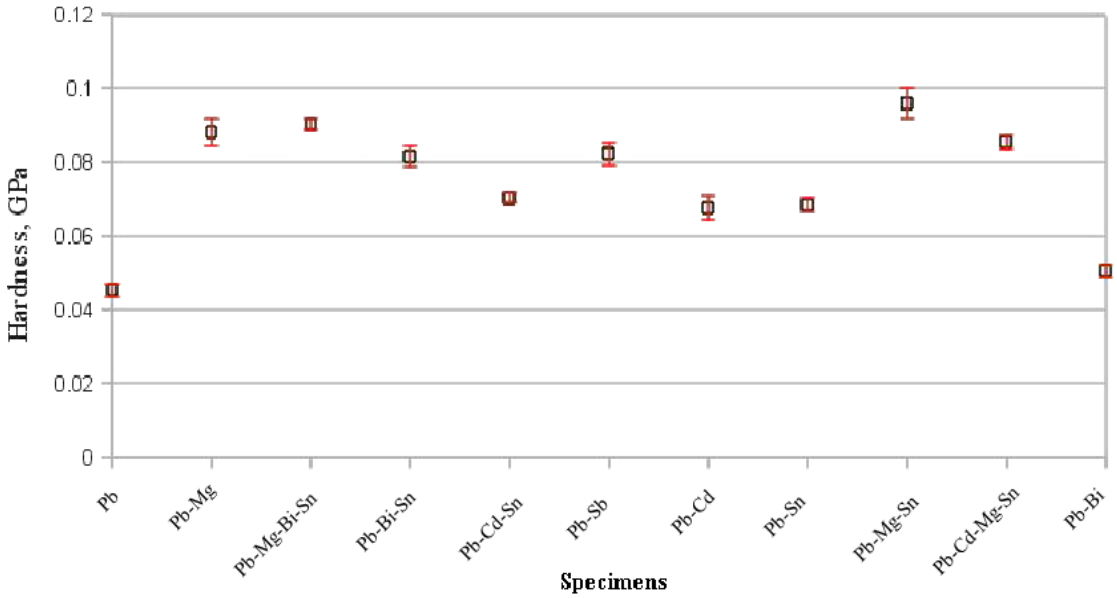

Figure 4.12 Hardness values of all specimens.

4.3 Corrosion Measurement

The corrosion measurements can be divided into three categories; open circuit potential (OCP), potentiodynamic polarization and polarization resistance measurements which include also computational corrosion rate calculations.

4.3.1 Open Circuit Potential (OCP) Measurements

The OCP measurements were carried out for 1 h and the OCP potentials of each alloy at 1 and 55 min are given in Table 4.1. Representative OCP curves are given in Figure 4.13 for a two alloy system.

As it can be seen from Figure 4.13 and Table 4.1, film layer was formed over time and passivation was occurring rapidly.

Table 4.1 OCP measurement results which were made before polarization resistance measurements.

Specimens	OCP(V) at 1 min.	OCP(V) at 55 min.
Pb	-0,600	-0,604
Pb-Bi	-0,620	-0,613
Pb-Cd	-0,619	-0,612
Pb-Mg	-0,595	-0,597
Pb-Sb	-0,604	-0,598
Pb-Sn	-0,594	-0,586
Pb-Bi-Sn	-0,604	-0,602
Pb-Cd-Sn	-0,595	-0,596
Pb-Mg-Sn	-0,603	-0,598
Pb-Cd-Mg-Sn	-0,616	-0,606
Pb-Mg-Bi-Sn	-0,616	-0,611

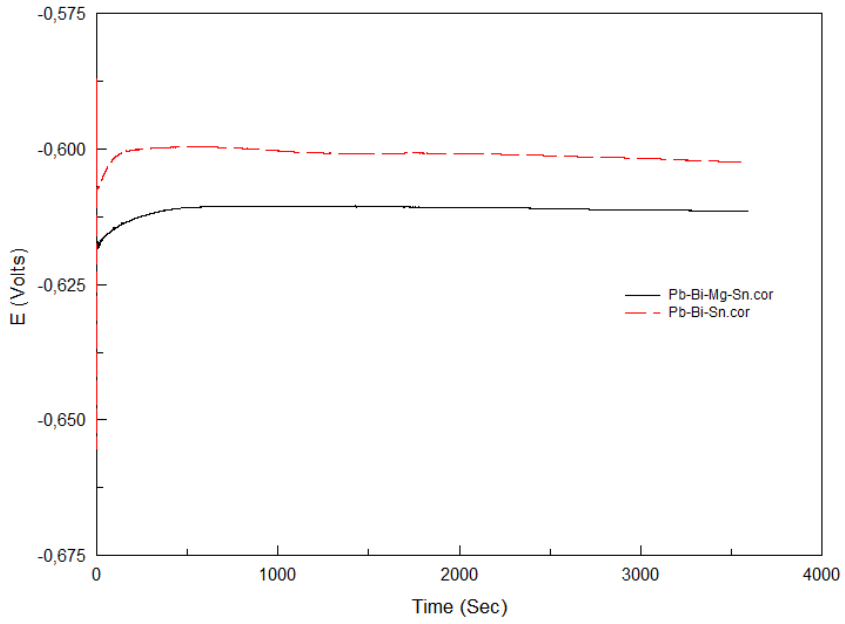

Figure 4.13 Representative OCP measurements results graph of Pb-Bi-Mg-Sn and Pb-Bi-Sn which were made before polarization resistance measurements.

4.3.2 Potentiodynamic Polarization Measurement

The purpose of the potentiodynamic polarization measurement was to determine primary passivation potential, E_{pp}, critical current density, $i_{critical}$, passive potential, E_p, and passivation current density, i_p. Passive film formed surface was tested in 3.75 M H_2SO_4 solution at room temperature. The Table 4.2 and Figure refers to 4.14 for showing a representative curve given below are showing variations with respect to primary passivation potential, critical current density, passive potential and passivation current density.

Table 4.2 Primary passivation potential, E_{pp}, critical current density, $i_{critical}$, passive potential, E_p, passivation current density, i_p, of specimens.

Specimens	E_{pp} **(volt)**	$i_{critical}$ **(amps/cm^2) (x10^{-3})**	E_p **(volt)**	i_p **(amps/cm^2) (x10^{-5})**
Pb	-0.5755	0.784	-0.525	7.353
Pb-Bi	-0.5797	0.725	-0.538	6.723
Pb-Cd	-0.5713	1.064	-0.527	8.588
Pb-Mg	-0.5760	1.220	-0.538	7.427
Pb-Sb	-0.5827	1.028	-0.548	11.401
Pb-Sn	-0.5695	0.667	-0.543	5.409
Pb-Bi-Sn	-0.5703	1.415	-0.534	5.702
Pb-Cd-Sn	-0.5734	1.485	-0.541	5.347
Pb-Mg-Sn	-0.5705	1.461	-0.533	5.354
Pb-Cd-Mg-Sn	-0.5767	1.398	-0.546	8.658
Pb-Mg-Bi-Sn	-0.5709	1.047	-0.544	9.316

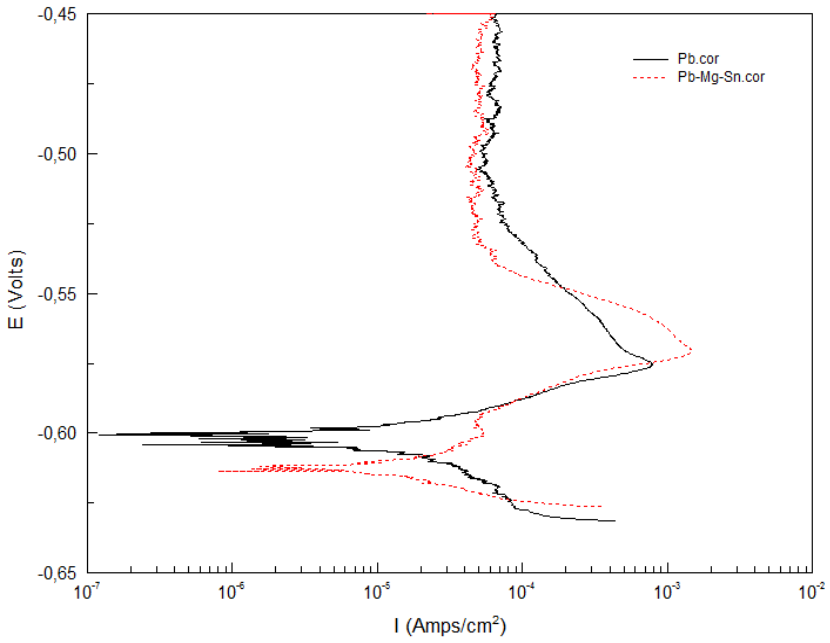

Figure 4.14 Representative view of primary passivation potential, E_{pp}, critical current density, $i_{critical}$, passive potential, E_p, passivation current density, i_p, of Pb and Pb-Mg-Sn specimens.

In accordance with the potentiodynamic polarization measurement results, critical current density values showed different characteristics; although, the passivation potentials varied in about – 0.57 Volt. The lowest $i_{critical}$ value was observed for pure Pb, Pb-Bi and Pb-Sn, which reached earlier passivation region than others. Their values almost 2 times lower than ternary alloys. In binary alloys, $i_{critical}$ value of Pb-Cd, Pb-Mg and Pb-Sb alloys showed almost the same characteristics. The values of ternary alloys in $i_{critical}$ and i_p were almost the same, so effect of the addition of Bi, Cd and Mg into Pb-Sn alloy was not much observable. In quaternary alloys, the addition of Cd and Bi to Pb-Mg-Sn resulted that in a decrese in $i_{critical}$ value compared to Pb-Mg-Sn. Among all specimens, ternary alloys exhibited the highest values for $i_{critical}$.

4.3.3 Polarization Resistance Measurement

The aim of linear polarization measurements was to characterize the corrosion behavior of the passive film formed surface. This measurement was made in a 3.75 M H_2SO_4 solution at RT. The obtained data was then fed to a computer program, fortran, to calculate the corrosion potentials, current densities and corrosion rates. The given representative Figures 4.15 and 4.16 below shows variations with respect to potential and current densities in the order of passive film formed surfaces.

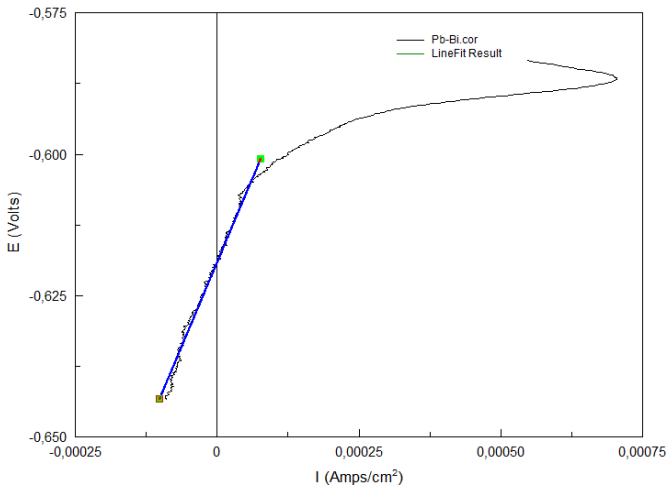

Figure 4.15 *E* vs *I* graph of pure Pb-Bi with passive film.

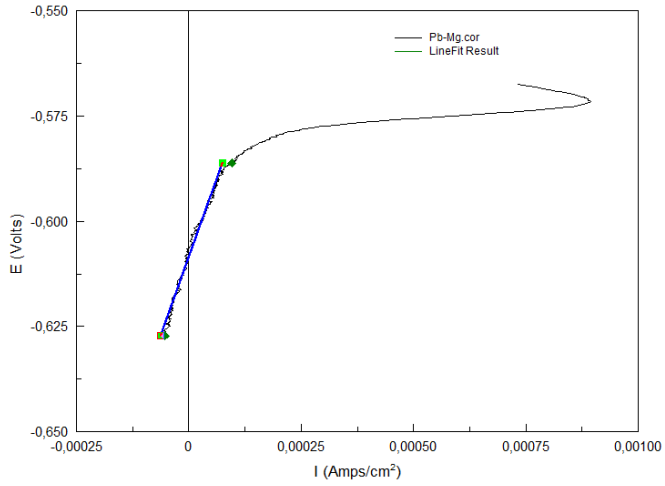

Figure 4.16 *E* vs *I* graph of pure Pb-Mg with passive film.

The computed corrosion potentials, current densities and corrosion rates are given in Table 4.3.

Table 4.3 The computational results of E_{corr}, I_{corr}, R_p, and corrosion rate, for all specimens with respect to passive film formed surface conditions.

Specimens	R_p	I_{corr} **(A/Cm^2)**	E_{corr} **(V)**	*Corrosion Rate* **(mm/year)**
Pb	32766.551	8.625E-07	-0.595	0.026
Pb-Bi	812.832	3.893E-05	-0.619	1.176
Pb-Cd	868.162	2.219E-05	-0.639	0.663
Pb-Mg	270227.031	1.042E-07	-0.587	0.003
Pb-Sb	924.972	1.917E-05	-0.611	0.573
Pb-Sn	698.907	2.714E-05	-0.591	0.811
Pb-Bi-Sn	1694.877	1.507E-05	-0.625	0.450
Pb-Cd-Sn	1040.876	1.885E-05	-0.610	0.563
Pb-Mg-Sn	934.574	3.305E-05	-0.609	0.988
Pb-Cd-Mg-Sn	873.881	3.753E-05	-0.609	1.121
Pb-Mg-Bi-Sn	1260.704	1.385E-05	-0.611	0.414

As shown in Figures 4.15 and 4.16, and taking into account Table 4.3, polarization diagrams, their results exhibited different corrosion behavior.

According to literature, intergranular corrosion generally occurs in VRLA batteries, and so enhanced corrosion resistance is expected with increasing grain size [27]. However, when grain size and corrosion rate of the alloys were compared each other, their values did not confirm literature. Hence, not only intergranular corrosion but also other corrosion types may occur in our specimens.

It was obvious that pure Pb is excellent in terms of corrosion rates. However, it is too soft and the passivation layer that forms on pure Pb grids can lead to premature drop in capacity of the battery during the first few cycles. The passive film completely covers the surface of the pure Pb grid [44] and the electrical conductivity of the passive layer is very low which poses some problems. Addition of Sn, commercially used in the production of positive and negative grids of VRLA batteries, to pure Pb have greatly diminished the problems occurred on cycling

batteries with grid made from this metal. Small amounts of Sn (0.3 - 0.6 wt. %) dramatically increase the charge acceptance of pure Pb. Also, Sn-containing corrosion layers are more conductive than those formed on pure Pb [44, 45].

It is reported in literature, [46] that Bi content less than 0.2 wt. % increases the corrosion rate. We have indeed obtained the highest corrosion rate in Pb-Bi alloy; however, by the addition of Sn, it decreased three times.

In binary alloys, Pb-Cd, Pb-Sb and Pb-Sn alloys have intermediate corrosion rates. Corrosion rate of Pb-Sb alloy is slightly lower than Pb-Cd alloy.

In literature there is no that of information about the use Pb-Mg alloys in battery grids. According to our results, its corrosion behavior was found to be superior as compared to other alloys. However, the effect of Mg is decreased in ternary and quadruple alloy systems.

In ternary alloy systems, corrosion rate of Pb-Bi and Pb-Cd alloys was decreased three times and a little bit, respectively, by the addition of Sn. In the case of Sn addition to Pb-Mg alloy, corrosion rate was dramatically increased from 0.003112 to 0.9875.

In quaternary alloy systems, while the Bi addition into Pb-Mg-Sn alloy decreases in the corrosion rate values, the Cd addition into Pb-Mg-Sn alloy increases the corrosion rate. Corrosion rate value of Pb-Mg-Sn alloy was as much as 300 times higher than that of Pb-Mg alloy, so that the effect of Sn was disappeared in Pb-Mg binary alloy.

When the corrosion potentials, E_{corr}, were examined, it was obvious that for pure Pb and Pb-Mg specimens, E_{corr} value was more noble than for other specimens.

4.4 Gas Evolution Measurement

The hydrogen evolution studies given in Figure 4.17 revealed that Pb-Bi and Pb-Cd alloys have the highest hydrogen gassing evolution among binary alloys. Actually, some of the studies in the literature report that addition of Bi does not increase the rate of hydrogen

evolution [31, 47]. But, according to Johnson et al. [48], presence of Bi in Pb could lead to an increase in the rate of hydrogen evolution in the range of 0-0.275 wt. %.

According to the literature, Sn is known decrease and Sb is known to increase the hydrogen gassing [47]. However, we have not seen much difference in the behavior of gassing evolution of Pb-Sn and Pb-Sb alloys. There is no information about Mg and Cd on hydrogen gassing behavior in the literature. As we have stated above, Cd has a similar effect like Bi, but Mg is found to have a superior effect on hydrogen gassing.

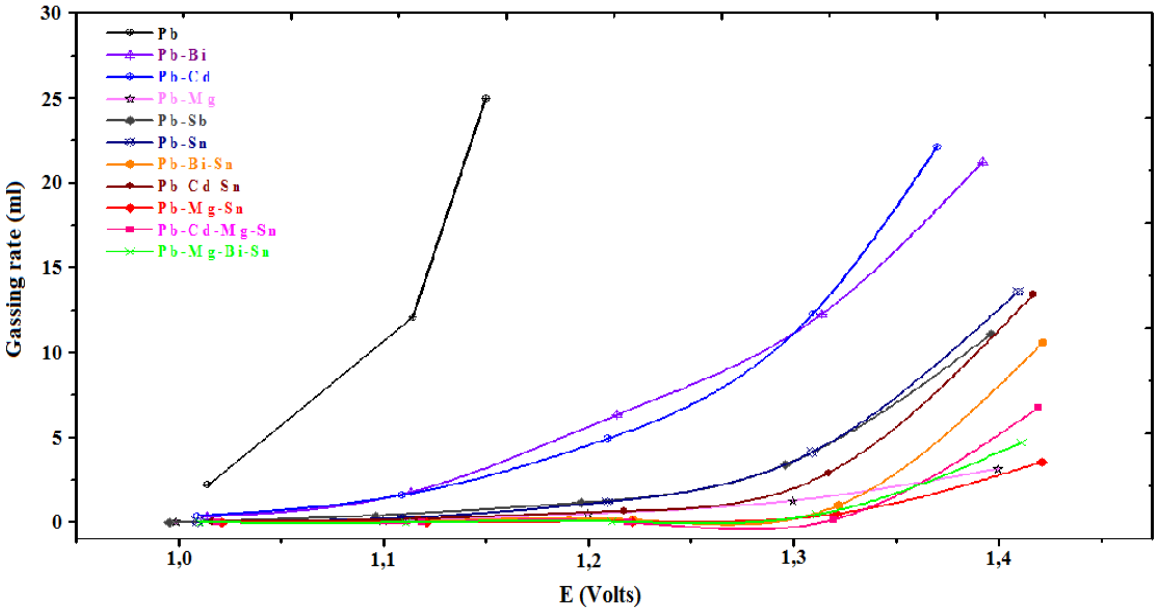

Figure 4.17 Hydrogen gassing evolution of specimens.

4.5 PbO Conductivity Measurement

In order to determine the role of alloying elements such as Bi, Cd, Mg, Sb, Sn on the conductivity of the passivation layer at the grid-lead dioxide interface, PbO conductivity measurement test was performed. Two passivation criteria, *R* is the intensity ratio and *C* is the peak area, have been investigated as shown in Figures 4.18 and 4.19. According to Miraglio [21] and Albert [20], as *R* and *C* values are close to one, the corrosion layer, mainly constituted by PbO, is supposed to be more conductive and the passivation is suppressed. This measurement results revealed that *R* and *C* values of Pb-Sn binary alloy are closer to one than other

specimens. This result may explain that passivation layer consists of an outer thin $PbSO_4$ film and a thick inner layer of tetragonal PbO (α-PbO) oxide which grows under deep-discharge conditions [49, 20]. Addition of Sn, as an alloying element, to the Pb raises the conductivity of the passivation PbO film and decreases the thickness of the PbO film. Because the thickness of the PbSO4 layer is found to be independent on the alloy composition whereas that of PbO layer is dependent on the Sn content [21, 50, 51]. It was reported in literature that, if the Sn amount is less than 1 wt. %, passivation layer is non-conducting. Sn content around 1-1.5 wt. % improves conductivity of passivation layer. The conductivity reaches a plateau for 1.5-2.5 wt. % Sn. Higher Sn content leads to a porous sulfate layer and the growth of the PbO layer is restrained [20, 49, 52].

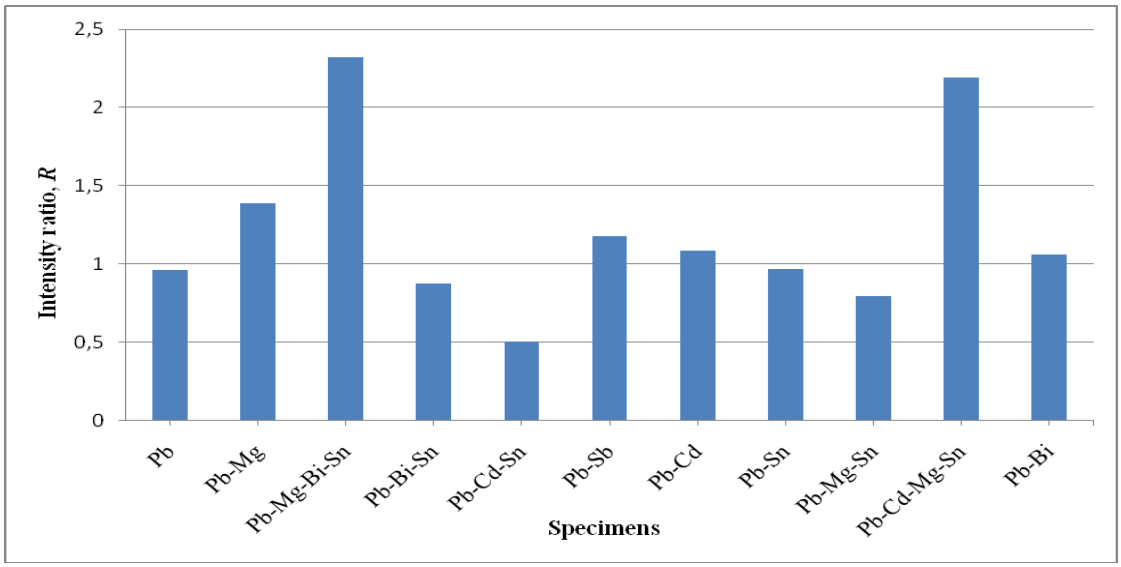

Figure 4.18 Development of *R* values.

According to our results, Mg-containing alloys did not show good conductivity characteristics due to higher oxidation tendency of Mg. However, its effect was decreased by the addition of Sn. The result obtained from Figure 4.19, *C* criteria, is not closely matching with the results in Figure 4.18, *R* criteria. This could be due to difficulties in the determination of the area of the PbO_2 to $PbSO_4$ reduction peak.

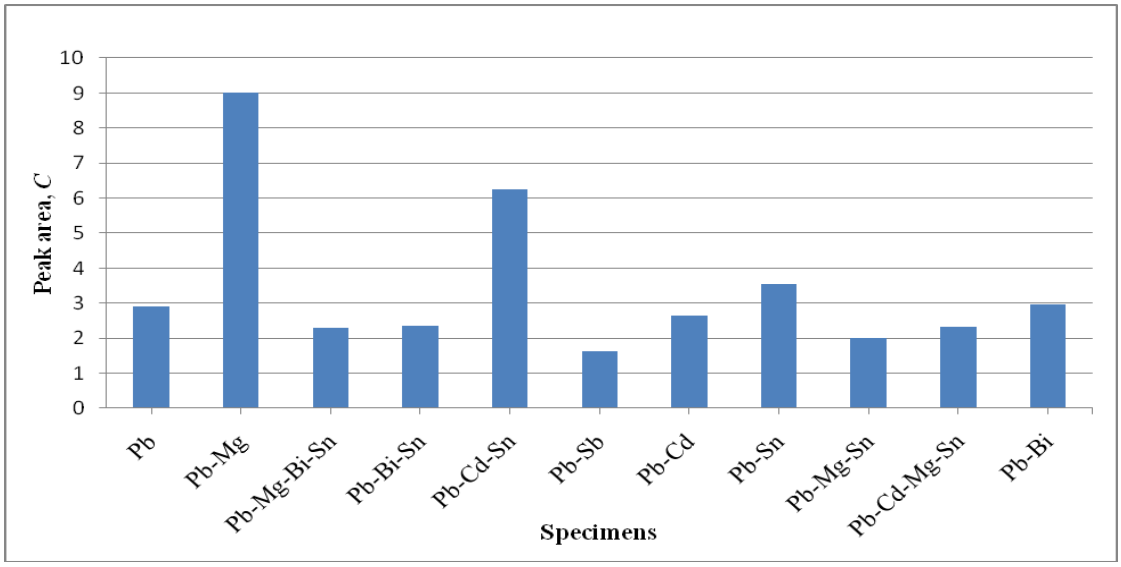

Figure 4.19 Development of *C* values.

CHAPTER 5

CONCLUSIONS

The purpose of this study was to investigate the hardness behavior and the corrosion resistance, conductivity of the passive film and gassing behavior of Pb alloys for VRLA batteries. For this purpose, Mg, Sn, Cd, Bi and Sb containing binary, ternary and quaternary alloys were prepared by melting and casting.

Hardness measurement results revealed that proper alloying addition to pure Pb increases the hardness of the alloys. The minimum hardness value was obtained in pure Pb and Pb-Bi alloy. Mg containing alloys have the highest hardness values among all.

Corrosion measurements exhibited that lowest $i_{critical}$ value was observed for Pb, Pb-Bi and Pb-Sn, which reached passivation region earlier than others. Passive film formation was seen for all specimens. E_{corr} value of Pb and Pb-Mg were more noble than others. Also, minimum corrosion rates belonged to Pb and Pb-Mg alloys.

Gassing evolution measurements showed that Pb-Bi and Pb-Cd have the highest evolution rate. There were not seen much difference in the behavior of gassing evolution of Pb-Sn and Pb-Sb alloys. Mg is found to have a superior effect on hydrogen gassing.

Conductivity measurements exhibited that the addition of 1-1.5 wt. % Sn as an alloying element, to the pure Pb increases the conductivity of the passivation layer. Mg containing alloys did not show good conductivity characteristics.

In conclusion, while Mg containing alloys showed promising properties in terms of corrosion behavior, gassing evolution and hardness behavior, conductivity of passivation layer

of that alloys gave undesired results. Even so Mg as an alloying element in Pb seems to have a future in the development of VRLA batteries.

As a future study, only Pb-Mg-Sn alloys can be investigated in detail with different amount of Mg and Sn. Conductivity of PbO film formed on grid can be examined by different methods such as electrochemical impedance spectroscopy, thickness and content of PbO film can be determined. In order to understand detailed microstructure of these alloys, TEM investigation can be carried out.

REFERENCES

[1] Kiehne, H.A., “Battery Technology Handbook”, Second ed., Marcel Dekker, NY, USA, pp. 1, 2003.

[2] Linden, D., “Basic Concepts”, in Handbook of Batteries, Linden, D., Reddy, T. B., Editors, Third ed., McGraw Hill, NY, USA, pp. 1.3-1.6, 2002.

[3] Tuck, C.D.S., “Modern Battery Technology”, Ellis Horwood, NY, USA, pp. 19, 1991.

[4] Nishio, K., Furukawa, N., “Practical Batteries”, in Handbook of Battery Materials, Besenhard, J.O., Editor, Wiley-VCH, NY, USA, pp. 47, 1999.

[5] Ehrlich, G.M., “Lithium-Ion Batteries”, in Handbook of Batteries, Linden, D., Reddy, T.B., Editors, Third ed., McGraw Hill, NY, USA, pp. 35.1-35.2, 2002.

[6] Bode, H., “Lead-Acid Batteries”, John Wiley & Sons, NY, USA, pp. 2-23, 1977.

[7] Dell, R.M., Rand, D.A.J., “Understanding Batteries”, Royal Society of Chemistry, Cornwall, UK, pp. 101, 2001.

[8] Salkind, A.J., Cannone, A.G., Trumbure, F.A., “Lead-Acid Batteries”, in Handbook of Batteries, Linden, D., Reddy, T.B., Editors, Third ed., McGraw Hill, NY, USA, pp. 23.6-23.29, 2002.

[9] Salkind, A.J., Hammel, R.O., Cannone, A.G., Trumbure, F.A., “Valve Regulated Lead-Acid Batteries”, in Handbook of Batteries, Linden, D., Reddy, T.B., Editors, Third ed., McGraw Hill, NY, USA, pp. 24.3, 2002.

[10] Crompton, T.R., “Battery Reference Book”, Third ed., Newnes, Oxford, UK, pp. 18.1, 2000.

[11] Warlimont, H., Hofmann, T., Jobst, K., “Superior corrosion properties and reduced cost of lead–acid batteries using electroformed grids“, Journal of Power Sources, v144, pp. 486-493, 2005.

[12] Berndt, D., “Valve-regulated lead-acid batteries”, Journal of Power Sources, v95, pp. 2-12, 2001.

[13] Culpin, B., Rand, D.A.J., “Failure modes of lead/acid batteries”, Journal of Power Sources, v36, pp. 429-431, 1991.

[14] Bose, C.S.C., Mathiesen, G.W., “Gas Evolution, Recombination and Grid Corrosion in a VRLA Battery Under High Temperature Operating Conditions”, Telecommunications Energy Conference, 1997. INTELEC 97., 19th International, Melbourne, Australia, pp. 13-17, 19-23 Oct. 1997.

[15] Lam, L.T., Lim, O.V., Haigh, N.P., Rand, D.A.J., Manders, J.E., Rice, D.M., “Oxide for valve-regulated lead-acid batteries”, Journal of Power Sources, v73, pp. 36-46, 1998.

[16] Guanfa, L., Genshu, Z., Dangguo, L., Maosheng, Z., “Effect of cerium on gas evolution behavior of Pb-Ca-Sn alloy”, Journal of Rare Earths, v24, pp. 232-237, 2006.

[17] Schenk, R.L., US Patent 5,601,953, 1997.

[18] Oerlikon Stationary Batteries Ltd., Corrosion Phenomena of Lead Alloys, Retrieved July 27, 2010, from http://www.accuoerlikon.com/lead-corrosion.htm.

[19] Shervedani, R.K., Isfahani, A.Z., Khodavisy, R., Hatefi-Mehrjardi, A., “Electrochemical investigation of the anodic corrosion of Pb–Ca–Sn–Li grid alloy in H_2SO_4 solution”, Journal of Power Sources, v164, pp. 890-895, 2007.

[20] Albert, L., Chabrol, A., Torcheux, L., Steyer, P., Hilger, J.P., “Improved lead alloys for lead/acid positive grids in electric-vehicle applications”, Journal of Power Sources, v67, pp. 257-265, 1997.

[21] Miraglio, R., Albert, L., Ghachcham, A.E., Steinmetz, J., Hilger, J.P., “Passivation and corrosion phenomena on lead-calcium-tin alloys of lead/acid battery positive electrodes”, Journal of Power Sources, v53, pp. 53-61, 1995.

[22] Tizpar, A., Ghasemi, Z., “Influence of silver on the anodic corrosion and gas evolution of Pb–Sb–As–Se alloys as positive grids in lead acid batteries”, Applied Surface Science, v252, pp. 7801-7808, 2006.

[23] Guo, W.X., Shu, D., Chen, H.Y., Li, A.J., Wang, H., Xiao, G.M., Dou, C.L., Peng, S.G., Wei, W.W., Zhang, W., Zhou, H.W., Chen, S., “Study on the structure and property of lead tellurium alloy as the positive grid of lead-acid batteries”, Journal of Alloys and Compounds, v475, pp. 102-109, 2009.

[24] Chen, H.Y., Li, S., Li, A.J., Shu, D., Li, W.S., Dou, C.L., Wang, Q., Xiao, G.M., Peng, S.G., Chen, S., Zhang, W., Wang, H., “Lead–samarium alloys for positive grids of valve-regulated lead–acid batteries”, Journal of Power Sources, v168, pp. 79-89, 2007.

[25] Li, A., Cheni, Y., Chen, H., Shu, D., Li, W., Wang, H., Dou, C., Zhang, W., Chen, S., “Electrochemical behavior and application of lead–lanthanum alloys for positive grids of lead-acid batteries”, Journal of Power Sources, v189, pp. 1204-1211, 2009.

[26] Li, D.G., Zhou, G.S., Zhang, J., Zheng, M.S., “Investigation on characteristics of anodic film formed on PbCaSnCe alloy in sulfuric acid solution”, Electrochimica Acta, v52, pp. 2146-2152, 2007.

[27] Mukaitani, I., Tsubakino, H., Liu, L., Yamamoto, A., Fukumoto, S., “Microstructural analysis of new lead–acid electrode alloys”, Journal of Power Sources, v158, pp. 897-901, 2006.

[28] Nuzhny, A., “Corrosion of low-antimony lead–cadmium alloys in conditions of long-term polarization”, Journal of Power Sources, v158, pp. 920–926, 2006.

[29] Jullian, E., Albert, L., Caillerie, J.L., “New lead alloys for high-performance lead–acid batteries”, Journal of Power Sources, v116, pp. 185–192, 2003.

[30] Liang, J.Z., Chen, H.Y., Tang, M.C., Wu, Y.M., Xiao, G.M., Zhou, H.W., Li, W.S., Jiang, X., “Properties and application of lead–calcium–tin–aluminium–bismuth alloys for positive grids”, Journal of Power Sources, v158, pp. 908-913, 2006.

[31] Wu, Y.M., Li, W.S., Long, X.M., Wu, F.H., Chen, H.Y, Yan, J.H., Zhang, C.R., “Effect of bismuth on hydrogen evolution reaction on lead in sulfuric acid solution”, Journal of Power Sources, v144, pp. 338–345, 2005.

[32] Massalski, T.B., Okamoto, H., “Binary Alloy Phase Diagrams”, Second ed., ASM International, Metals Park, OH, USA, 1990.

[33] Revie, R.W., Uhlig, H.H., “Corrosion and Corrosion Control”, Fourth Ed., John Wiley Sons, NJ, USA, pp.1, 2008

[34] Jones, D.A., "Principles and Prevention of Corrosion", Second ed. Upper Saddle River, NJ 07458, Prentice Hall, pp. 4, 1996.

[35] Topçuoğlu, M., "Microstructural and Electrochemical Characterization of Ti-6Al-4V Eli Alloy", M.S. Thesis, Department of Metallurgical and Materials Engineering, Middle East Technical University, Ankara, 2006.

[36] Davis, J.R., “Corrosion Understanding the Basics”, ASM International, Materials Park, OH, USA, pp. 53-54, 2000.

[37] Stansbury, E.E., Buchanon, R.A., “Fundamentals of Electrochemical Corrosion”, ASM International, Materials Park, OH, USA, pp. 45, 2000.

[38] Perez, N., “Electrochemistry and Corrosion Science”, Kluwer Academic Publishers, Dordrecht, Netherlands, pp. 71-92, 2004.

[39] Talbot, D., Talbot, J., “Corrosion Science and Technology”, CRC Press, USA, pp. 3.2.2.2, 1998.

[40] Ahmed, Z., “Principles of Corrosion Engineering and Corrosion Control”, Elsevier Science and Technology Books, pp. 94-98, 2006.

[41] Scully, J.R., “Electrochemical Methods of Corrosion Testing”, In Corrosion, v13, Laboratory Testing, Ninth Ed., ASM International, Materials Park, OH, USA, pp. 236, 1987.

[42] Mansfeld, F., "Simultaneous determination of corrosion rates and tafel slopes from polarization resistance measurements", Journal of Electrochemical Society, v120, pp. 515, 1973.

[43] Gilman, J.J., “Chemistry and Physics of Mechanical Hardness”, John Wiley & Sons, NY, USA, pp. 94, 2009.

[44] Rand, D.A.J., Moseley, P.T., Garche, J., Parker, C.D., “Valve Regulated Lead Acid Batteries”, Elsevier Science and Technology Books, pp. 15-16, 2004.

[45] Peixoto, L.C., Osorio W.R., Garcia A., “Microstructure and electrochemical corrosion behavior of a Pb-1 wt. % Sn alloy for lead-acid battery components”, Journal of Power Sources, v192, pp. 724–729, 2009.

[46] Koop, M.J., Rand, D.A.J., Culpin, B., “A Guide to the influence of bismuth on lead/acid battery performance”, Journal of Power Sources, v45, pp. 365–377, 1993.

[47] Huang, A.H., Windsor, J.C., Manders, J.E., Bui, N., Lambert, D.W.H., Navarette, J., Nelson, R.F., Valeriote, E.M., “Lead/acid battery design and operation”, Journal of Power Sources, v73, pp. 152–161, 1998.

[48] Johnson, M., Ellis, S.R., Hampson, N.A., Wilkinson, F., Ball, M.C., “The hydrogen evolution reaction on lead-bismuth alloys”, Journal of Power Sources, v22, pp. 11-20, 1988.

[49] Amrani, A.E.G., Steyer, P., Steinmetz, J., Delacroix, P., Caër, G.L., “Analysis of tin lead oxide by mössbauer spectrometry and transmission electron microscopy”, Journal of Power Sources, v64, pp. 35–37, 1997.

[50] Giess, H.K., “Advances in Lead-Acid Batteries”, Proceeding Vol. 84-14, Bullock, K. P., Pavlov, D., Editors, The Electrochemical Society, Pennington, NJ, USA, p. 241, 1984.

[51] Döring, H., Garche, J., Dietz, H., Wiesener, K., “Currentless passivation of the PbO_2 electrode with respect to the influence of tin”, Journal of Power Sources, v30, pp. 41-45, 1990.

[52] Simon, P., Bui, N., Dabosi, F., “An in situ study of the effect of tin on the passivation of lead-tin Alloys”, Journal of Power Sources, v50, pp. 141-152, 1994.